

# JGR Planets

## RESEARCH ARTICLE

10.1029/2019JE006304

### Special Section:

Investigations of Vera Rubin Ridge, Gale Crater

### Key Points:

- The Sample Analysis at Mars instrument suite studied carbon-sulfur gases released during evolved gas analysis of Vera Rubin ridge samples
- Quadratic discriminant analysis compared laboratory and flight data to identify Martian samples that contain reduced sulfur
- Two Vera Rubin ridge samples from the Jura member were identified as likely to include reduced sulfur

### Supporting Information:

- Supporting Information S1

### Correspondence to:

G. M. Wong,  
gkw5061@psu.edu

### Citation:







Wong, G. M., Lewis, J. M. T., Knudson, C. A., Millan, M., McAdam, A. C., Eigenbrode, J. L., et al. (2020). Detection of reduced sulfur on Vera Rubin ridge by quadratic discriminant analysis of volatiles observed during evolved gas analysis. *Journal of Geophysical Research: Planets*, 125, e2019JE006304. <https://doi.org/10.1029/2019JE006304>

Received 29 NOV 2019

Accepted 19 MAY 2020

Accepted article online 10 JUN 2020

## Detection of Reduced Sulfur on Vera Rubin Ridge by Quadratic Discriminant Analysis of Volatiles Observed During Evolved Gas Analysis

Gregory M. Wong<sup>1</sup> , James M. T. Lewis<sup>2,3,4</sup>, Christine A. Knudson<sup>3,4,5</sup> , Maëva Millan<sup>3,6</sup>, Amy C. McAdam<sup>3</sup> , Jennifer L. Eigenbrode<sup>3</sup> , Slavka Andrejkovičová<sup>3</sup>, Felipe Gómez<sup>7</sup> , Rafael Navarro-González<sup>8</sup>, and Christopher H. House<sup>1</sup> 

<sup>1</sup>Department of Geosciences, Pennsylvania State University, University Park, PA, USA, <sup>2</sup>Department of Physics and Astronomy, Howard University, Washington, DC, USA, <sup>3</sup>Planetary Environments Laboratory, NASA Goddard Space Flight Center, Greenbelt, MD, USA, <sup>4</sup>Center for Research and Exploration in Space Science and Technology, NASA GSFC, Greenbelt, MD, USA, <sup>5</sup>Department of Astronomy, University of Maryland, College Park, MD, USA, <sup>6</sup>Department of Biology, Georgetown University, Washington, DC, USA, <sup>7</sup>Centro de Astrobiología (CSIC-INTA), Torrejón de Ardoz, Madrid, Spain, <sup>8</sup>Instituto de Ciencias Nucleares, Universidad Nacional Autónoma de México, Ciudad Universitaria, Ciudad de México, Mexico

**Abstract** The Mars Science Laboratory mission investigated Vera Rubin ridge, which bears spectral indications of elevated amounts of hematite and has been hypothesized as having a complex diagenetic history. Martian samples, including three drilled samples from the ridge, were analyzed by the Sample Analysis at Mars instrument suite via evolved gas analysis-mass spectrometry (EGA-MS). Here, we report new EGA-MS data from Martian samples and describe laboratory analogue experiments. Analyses of laboratory analogues help determine the presence of reduced sulfur in Martian solid samples, which could have supported potential microbial life. We used evolved carbonyl sulfide (COS) and carbon disulfide (CS<sub>2</sub>) to identify Martian samples likely to contain reduced sulfur by applying a quadratic discriminant analysis. While we report results for 24 Martian samples, we focus on Vera Rubin ridge samples and select others for comparison. Our results suggest the presence of reduced sulfur in the Jura member of Vera Rubin ridge, which can support various diagenetic history models, including, as discussed in this work, diagenetic alteration initiated by a mildly reducing, sulfite-containing groundwater.

**Plain Language Summary** The Mars Science Laboratory studied the chemical composition of Vera Rubin ridge in Gale crater, Mars. The Sample Analysis at Mars, a set of scientific instruments designed to study rock chemistry, observed a number of gases released during the heating of Martian drilled samples. The same gases were observed when Mars-relevant minerals were analyzed with similar instruments on Earth. From these two sets of data, we applied statistical analyses to determine which Mars samples on Vera Rubin ridge contained important sulfur compounds. Two samples on the ridge showed evidence for these compounds, which could have supported the energetic requirements for life. The results presented here improve both the understanding of the history of Gale crater and the potential for ancient life to have existed.

## 1. Introduction

### 1.1. Mars Science Laboratory Mission and Vera Rubin Ridge

The Mars Science Laboratory (MSL) Curiosity rover has been exploring Gale crater, Mars, since landing in 2012. Gale crater, an ~155 km diameter impact crater, is located near the Martian crustal dichotomy and contains some of the lowest elevations in the southern hemisphere (Wray, 2013). Within Gale crater is Aeolis Mons (informally known as Mount Sharp), which hosts ~5 km of stratified deposits that recorded Martian geological and environmental history (Grotzinger & Milliken, 2012). Evidence from orbit indicates a geologic record of ancient aqueous environments and varying mineralogy that include phyllosilicates, sulfates, and hematite (Milliken et al., 2010). Gale crater was the chosen MSL landing site to investigate the variation and extended stratigraphy further.

One of the primary goals of MSL is to investigate Gale crater for evidence of past habitability while characterizing the crater's geology (Grotzinger et al., 2012). To this end, MSL has instrumentation to determine the presence of ancient liquid water, organic carbon, and redox gradients by analyzing the chemistry and mineralogy of Martian samples. Hundreds of meters of Gale's stratigraphy have been explored, and it has been found that there are mineralogically diverse sedimentary rocks that largely consist of mudstones and sandstones (Figure S1 in the supporting information). Early in the mission, it was determined that a habitable fluvio-lacustrine environment persisted at Gale crater—including fresh liquid water with a circumneutral pH and nonequilibrium mineral assemblages that included oxidized and reduced iron minerals (Grotzinger et al., 2014). As the Curiosity rover has ascended Mount Sharp, additional analyses have found evidence of native Martian organics, including chlorohydrocarbons (Freissinet et al., 2015) and recalcitrant organosulfur compounds (Eigenbrode et al., 2018).

One interesting geomorphological feature of Gale crater is a 200 m wide ridge with a strong spectral signature for hematite, now referred to as Vera Rubin ridge (VRR). Understanding the formation environments for the hematite-capped ridge is important for its implications in the broader context of Martian paleoenvironments, particularly in Gale crater. Previous studies about VRR focused on orbital data and two endmember models for the ridge's formations were derived from these data sets (Fraeman et al., 2013, 2016). The first proposed model by Fraeman et al. (2013) is that the hematite was authigenic and deposited from a redox interface of underlying Fe(II) from groundwater with atmospherically sourced oxidants. Their second model proposes that the hematite formed through interactions between diagenetic fluids in which dissolved Fe(II) came into contact with a second, oxidized fluid and precipitated out as hematite. These fluids would have been controlled by stratigraphy and porosity. Additional analyses performed by MSL allow for a more detailed understanding of VRR than from orbital data alone.

The Curiosity rover explored VRR from sol 1809 to 2302. VRR has been divided into two informal geologic members: Pettegrove Point member and Jura member (Figure S1). Jura is stratigraphically above Pettegrove Point and both members consist primarily of finely laminated mudstones. While the VRR members form a ridge, observations by MSL indicate that VRR is a continuation of the Murray Formation, which consists of hundreds of meters of finely laminated mudstones (Fedo et al., 2019). Additional observations indicate that VRR experienced several diagenetic events. For example, the Jura member consists of red and gray patches whose boundaries are not stratigraphically defined, which is suggestive of alteration (Horgan et al., 2019). Variations in Li and Mn content on VRR also suggest the flow of diagenetic fluids through VRR at some point in its history (Frydenvang et al., 2019). Data from the Sample Analysis at Mars (SAM) can be used to better understand diagenesis on VRR, including the ridge's redox history.

### 1.2. SAM Sulfur Volatile Findings

The SAM is an instrument suite on MSL that measures volatile compounds evolved from samples, which complements geological interpretations by other MSL instruments. SAM includes a pyrolysis oven and a gas chromatograph coupled to a mass spectrometer. Using these instruments, SAM can perform evolved gas analysis-mass spectrometry (EGA-MS) for solid sample analysis and gas chromatography-mass spectrometry (GC-MS) for separation and identification of organic and inorganic molecules (Mahaffy et al., 2012). EGA is a sensitive technique that is able to detect volatiles evolved during the ramped heating of solid samples. Previous EGA work has found evidence of both oxidized and reduced sulfur in the forms of SO<sub>2</sub> and H<sub>2</sub>S (and lesser COS and CS<sub>2</sub>) in both eolian materials and drilled samples of sedimentary rocks (Archer et al., 2014; Leshin et al., 2013; McAdam et al., 2014; Stern, Sutter, et al., 2018; Sutter et al., 2017). One explanation for the evolution of oxidized and reduced sulfur from a single sample is the presence of a sulfur mineral assemblage that is not in redox equilibrium. Reactions that occur in the oven during EGA can also affect the composition and/or oxidation state of evolved sulfur compounds. Either way, there is an indication that there is a source of reducing power in the Martian samples. While SO<sub>2</sub> is by far the most abundant evolved sulfur-bearing volatile, followed by H<sub>2</sub>S, there are other minor sulfur gases that can contain important redox information about a sample, such as carbonyl sulfide (COS) and carbon disulfide (CS<sub>2</sub>).

### 1.3. Carbon-Sulfur Volatiles From Sulfides

Carbon-sulfur gases can be telling of sample composition. A variety of carbon-sulfur gases (e.g., COS, CS<sub>2</sub>, CH<sub>3</sub>SH, and C<sub>2</sub>H<sub>6</sub>S) observed at high temperature during EGA in SAM have indicated the presence of

organosulfur compounds (Eigenbrode et al., 2018). The high-temperature observations of these gases have been interpreted as either breakdown products of larger molecules or the result of oven reactions. Carbon-sulfur gases have also been predicted and observed during coal pyrolysis, particularly at high temperature ( $>500^{\circ}\text{C}$ ), as a result of reactions between iron sulfides and carbon species (Attar, 1978). COS has especially been investigated and found to be produced during coal pyrolysis in significant amounts when  $\text{CO}_2$  is the carrier gas, but not with  $\text{N}_2$  carrier gas (Duan et al., 2009; Frigge et al., 2016). Production of COS can be the result of gas phase interactions in which CO or  $\text{CO}_2$  reacts with  $\text{H}_2\text{S}$ , or COS can be produced by a series of solid-gas interactions by reaction between  $\text{FeS}_2$  and  $\text{CO}_2$  (Arutyunov, 1992; Bhargava et al., 2009). The enhanced production of COS in  $\text{CO}_2$  carrier gas (compared to  $\text{N}_2$  carrier gas) suggests that  $\text{CO}_2$  can serve as a carbon source for carbon sulfur volatiles during pyrolysis. While most production of COS occurs at high temperature during coal pyrolysis, COS has been observed at temperatures below  $600^{\circ}\text{C}$  (Shao et al., 1994) and even as low as  $250^{\circ}\text{C}$  (Wang et al., 2014). Shao et al. (1994) also suggested that the production of COS competes with the production of  $\text{CS}_2$  from  $\sim 350^{\circ}\text{C}$  to  $900^{\circ}\text{C}$ .  $\text{CS}_2$  can form from gas-phase reactions between COS and COS,  $\text{H}_2\text{S}$  and COS, or C and  $\text{S}_2$ . While less frequently discussed compared to COS,  $\text{CS}_2$  is a common coal pyrolysis product (Attar, 1978) and has also evolved during EGA of numerous Martian samples (Eigenbrode et al., 2018; Leshin et al., 2013; McAdam et al., 2014). Though coal pyrolysis describes different samples than Mars (notably, coal has abundant organic carbon), the production of COS and  $\text{CS}_2$  by reduced sulfur and carbon interactions during coal pyrolysis can inform about possible related sulfur reactions during EGA with SAM. The significance of the production of these gases, particularly at lower temperatures, requires further examination. These volatiles can be used to study complex Martian samples and aid in determining the redox history of sites on Mars.

This paper presents a novel analysis of EGA data to aid in the identification of Martian samples that may contain reduced sulfur. We tested a range of volatile-bearing one or two component mixtures in laboratory SAM-like EGA. The EGA results from those experiments were used as training data for a multivariate analysis in which the relationships among COS,  $\text{CS}_2$ ,  $\text{SO}_2$ ,  $\text{CO}_2$ , and bisilylated water (BSW; a tracer of the organic derivatization agent N-Methyl-N-tert-butyl-dimethylsilyl-trifluoroacetamide, that is, MTBSTFA, in the SAM) were analyzed to discriminate between samples containing sulfides and sulfates. The laboratory work has direct implications to Mars, especially the presence/absence of reduced sulfur in the drilled samples of VRR, and can inform about the diagenetic history and potential habitability of the ridge.

## 2. Materials and Methods

### 2.1. SAM Evolved Gas Analysis-Mass Spectrometry

The operation of EGA on SAM has been described previously (Glavin et al., 2013; Mahaffy et al., 2012; Sutter et al., 2017). Briefly, solid samples—either drilled or scooped—are delivered to a pyrolysis oven. Samples are heated under a constant flow (0.8 ml/min) of helium at 25 mbar from  $\sim 30^{\circ}\text{C}$  to  $\sim 850^{\circ}\text{C}$  at a temperature ramp rate of  $35^{\circ}\text{C}/\text{min}$ . Volatiles released from the sample are carried by the He flow to the quadrupole mass spectrometer, which identifies mass-to-charge ratios ( $m/z$ ) of the ionized volatiles over the entire temperature range. These data are stored and converted into pyrograms that show intensity (counts per second) versus temperature.

### 2.2. Laboratory Experiments

We used a SAM-like EGA instrument setup at the NASA Goddard Space Flight Center to analyze the majority of the samples for this work. This setup used an Agilent 5975T-LTM MS attached to a Frontier PY-3030D pyrolysis oven. Powdered samples (section 2.3) were contained in organically clean stainless steel cups. Sample cups were dropped into the pyrolysis oven and kept at  $75^{\circ}\text{C}$  for up to 31 min (depending on the oven program) under a constant flow ( $\sim 50$  ml/min) of He at 30 mbar to allow for the desorption of adsorbed water from the sample. Cups were then heated linearly at  $35^{\circ}\text{C}/\text{min}$  until the oven temperature reached at least  $850^{\circ}\text{C}$  (SAM-like). The He flow carried volatiles produced during thermal decomposition to the mass spectrometer. The MS monitored up to  $m/z$  200, which covers the range of masses of the species expected to be detected. While the laboratory instrument setup is not exactly the same as SAM, the conditions used during EGA are selected to be comparable to SAM conditions and different SAM-like setups are frequently used to compare samples to SAM data (e.g., Glavin et al., 2013; McAdam et al., 2014; Ming et al., 2014). The major

**Table 1**  
*Compounds Used in Laboratory EGA*

| Sulfur compounds       |  | Nonsulfur compounds for mixtures |  |
|------------------------|--|----------------------------------|--|
| Pyrite <sup>a</sup>    | FeS <sub>2</sub>   | Halite                           | NaCl   |
| Troilite <sup>b</sup>  | FeS  | Calcium chloride                 | CaCl <sub>2</sub>  |
| Ferric sulfate Hydrate | Fe <sub>2</sub> (SO <sub>4</sub> ) <sub>3</sub> •nH <sub>2</sub> O | Magnesium chloride               | MgCl <sub>2</sub>  |
| Jarosite <sup>c</sup>  | KFe <sub>3</sub> (SO <sub>4</sub> ) <sub>2</sub> (OH) <sub>6</sub> | Calcium perchlorate              | Ca(ClO <sub>4</sub> ) <sub>2</sub>   |
| Kieserite <sup>d</sup> | MgSO <sub>4</sub> •H <sub>2</sub> O                                | Iron (III) perchlorate           | Fe(ClO <sub>4</sub> ) <sub>3</sub>   |
| Melanterite            | FeSO <sub>4</sub> •7H <sub>2</sub> O                               | Magnesium perchlorate            | Mg(ClO <sub>4</sub> ) <sub>2</sub>   |
|                        |  | Nontronite <sup>e</sup>          | (Ca <sub>0.5</sub> ,Na)Fe <sub>2</sub> (Si,Al) <sub>4</sub> O <sub>10</sub> (OH) <sub>2</sub> •nH <sub>2</sub> O |
|                        |  | Magnetite                        | Fe <sub>3</sub> O <sub>4</sub>   |
|                        |  | Siderite                         | FeCO <sub>3</sub>  |
|                        |  | MTBSTFA-DMF                      | C <sub>9</sub> H <sub>18</sub> F <sub>3</sub> NOSi - C <sub>3</sub> H <sub>7</sub> NO                            |
|                        |  | Magnesium acetate                | C <sub>4</sub> H <sub>6</sub> MgO <sub>4</sub>   |
|                        |  | Iron (III) oxalate               | C <sub>6</sub> Fe <sub>2</sub> O <sub>12</sub>   |
|                        |  | Myristic (tetradecanoic) acid    | C <sub>14</sub> H <sub>28</sub> O <sub>2</sub>   |

Note. All compounds were synthetic and purchased from Sigma-Aldrich except those marked with exceptions.

<sup>a</sup>Natural samples from Ward's Science and synthetic sample from Sigma-Aldrich. <sup>b</sup>Alfa Aesar. <sup>c</sup>Synthesized accord to method by Driscoll and Leinz (2005).

<sup>d</sup>ESTA. <sup>e</sup>Natural, Clay Minerals Society Source Clay NAu-2 from Uley Mine, Australia.

difference in EGA conditions is the high flow rate and split ratio used in the laboratory, which is necessary when running sulfur- and chlorine-rich samples to preserve instrument integrity.

### 2.3. Sample Preparation

Six inorganic sulfur-bearing compounds were used, including two sulfides (pyrite and troilite) and four sulfates (kieserite, jarosite, melanterite, and ferric sulfate hydrate). Refer to Table 1 for details on all compounds used. Ferric sulfate hydrate, kieserite, melanterite, and one pyrite sample were purchased from Sigma-Aldrich. All other pyrite samples were drilled out from a natural pyrite source (Ward's Science) and confirmed pure by X-ray diffraction (XRD; Terra<sup>®</sup> by inXitu, Inc., Campbell, CA; crystalline detection limit 1 wt.% or better; Blake et al., 2012). The jarosite was produced according to the protocol of Driscoll and Leinz (2005), and purity was confirmed by Terra XRD. FeS was from Alfa Aesar, stored in a desiccator, and >98 wt.% troilite/pyrrhotite and ~2 wt.% Fe metal according to Terra XRD. All solid samples were sieved to <150 μm grain size to simulate the size fractions analyzed with SAM. Samples were weighed and mixed with an inert, organically clean fused silica (Conrad et al., 2012; <150 μm) to physically disperse the sulfur minerals to simulate their natural occurrences where they are found within a matrix of other minerals. By mass, the ratio of sulfur compound to fused silica was ~9:1 in a given mixture. Mixing occurred either in bulk by mortar and pestle for 3 min or in individual sample cups with an inert, organically clean stainless-steel mixing tool. Samples were prepared at room temperature and atmospheric pressure. This is a difference from Martian samples, which are under Martian conditions (i.e., <10 mbar CO<sub>2</sub>-dominated atmosphere and cold temperatures) before delivery to SAM. Additionally, much more sulfur was used in the laboratory analyses (~10 wt.%) compared to the sulfur content observed in much more heterogeneous Martian samples (~2–5 wt.% SO<sub>3</sub>; Sutter et al., 2017). Due to the differences in laboratory and SAM analyses, the results of the laboratory EGA experiments are not exact replicas of Martian samples. Rather, these experiments allow us to explore the products of sulfur pyrolysis from simple, controlled mixtures in order to better describe the complex Martian mixtures.

In addition to the sulfur compounds alone in fused silica, mixtures were made with an ~10:1 mass ratio of sulfur to nonsulfur components except where otherwise noted. For a given sulfur/fused silica mixture, one of the following compounds was added in aqueous solution: sodium chloride, magnesium chloride, calcium chloride, calcium perchlorate, magnesium perchlorate, or iron (III) perchlorate (see Table 1). These Cl-bearing compounds, representing compounds present or potentially present on Mars, tested effects of HCl evolution and O<sub>2</sub> production on the evolution of sulfur-bearing volatiles. Mixtures of nontronite and magnetite with sulfur phases (1:1:1 ratio by mass) were used to test effects of possible H<sub>2</sub> production on sulfur evolution. To test the effects of carbon/sulfur redox on sulfur volatile evolution, mixtures of oxidized or reduced sulfur with either siderite (1:1) magnesium acetate (1:1), ferric oxalate (1:1), or myristic acid (sulfur to myristic acid by mass, 10:1) were used.



One additional experiment accounts for background MTBSTFA and dimethylformamide (DMF) that is in the SAM system. MTBSTFA is a derivatization compound used for SAM wet chemistry experiments. At least one of the cups containing MTBSTFA leaked into the SAM Sample Manipulation System (SMS) and produces low level background during analysis (Glavin et al., 2013). To investigate the effects of this reduced carbon contamination and potential mass interferences with COS and CS<sub>2</sub>, MTBSTFA-DMF (4:1) was added to select samples of oxidized and reduced sulfur in the laboratory in an ~100:1 mass ratio of sulfur to MTBSTFA. MTBSTFA readily reacts with hydroxyl groups and can produce a range of byproducts, including 1,3-bis(1,1-dimethylethyl)-1,1,3,3-tetramethyldisiloxane (BSW). BSW is detected in all Martian samples (Eigenbrode et al., 2018) and was used in this work as a tracer for MTBSTFA.

The presence of MTBSTFA acts as a confounding factor in the determination of reduced sulfur presence for two reasons. First, MTBSTFA is a large organic compound that can potentially act as a reducing agent during pyrolysis, increasing the amount of COS and CS<sub>2</sub> through reactions with sulfates. The second reason is that MTBSTFA can produce fragments or reaction byproducts that have interfering *m/z* values with COS and CS<sub>2</sub>. We tested several samples and mixtures with exposure to MTBSTFA to look at the derivatization agent's effects on the relevant volatiles used in the analysis. Included in these experiments were the four melanterite standards examined by the flight module (see below), the two CB analogue samples (see below), and five SAM-like EGA laboratory samples. These samples addressed the role of MTBSTFA, its byproducts, and its reactions in the QDA.

In addition to the laboratory experiments, we analyzed four samples of melanterite in the SAM flight module and two FeS-bearing mixtures in the SAM testbed. The melanterite standards were analyzed in the SAM flight module prior to launch and have been used as calibration standards for abundance calculations (Archer et al., 2014). The FeS-bearing mixtures were analyzed in the SAM testbed, a complete replica of the SAM flight model housed in a Mars simulation chamber (Malespin et al., 2016). These two samples were from the Cumberland Analogue (Knudson et al., 2018; Stern, Graham, et al., 2018), a mixture of analogue materials that simulates the mineralogy of the MSL Cumberland drill sample from the Sheepbed mudstone (Vaniman et al., 2014).

### 3. Data Processing and Analysis

#### 3.1. Volatile Areas

EGA data were processed in WaveMetrics IGOR Pro v6.0. Each run was deadtime (time between scans of different masses) corrected followed by a background subtraction. Data were then smoothed twice with an 11-point and subsequent 21-point moving average to reduce noise and ensure peaks are not a result of random background (Eigenbrode et al., 2018). After these corrections and smoothing, negative values were removed. Area under the curve (AUC) was calculated for each of the following volatiles from 75°C to 600°C: SO<sub>2</sub> (*m/z* 64), CO<sub>2</sub> (*m/z* 44), COS (*m/z* 60), CS<sub>2</sub> (*m/z* 76), and BSW (*m/z* 147). For the SAM data, SO<sub>2</sub> (*m/z* 64) and CO<sub>2</sub> (*m/z* 44) frequently saturate the detector. Due to this saturation, isotopologues were used: *m/z* 66 for SO<sub>2</sub> and *m/z* 45 for CO<sub>2</sub>. The amounts of *m/z* 64 and *m/z* 44 were calculated by multiplying the areas for the isotopologues by 20.39 and 83.25, respectively, which are the relative ratios of the isotopologues according to the National Institute of Standards and Technology (NIST Mass Spectrometry Data Center & Wallace, 2018). Temperatures for samples from pyrolysis oven 2 used the “oven-2\_model-1” model, which differs from some previous work due to ongoing model refinements (see McAdam et al., 2020 for more details). Due to the variation of integrated counts among different mixtures from oven reactions, statistical noise, differences in background subtractions, and smoothing parameters, the errors of associated integrated counts is estimated conservatively to be 20% for any count, consistent with previously reported EGA work (McAdam et al., 2014).

#### 3.2. Quadratic Discriminant Analysis

Quadratic discriminant analysis (QDA) is a multivariate, supervised machine-learning technique that is used to cluster unknown samples within a group based on known training variables. Other statistical methods, such as principal component analysis, aim to make interpretation of multivariate data sets simpler by reducing a data set's dimensionality to variables that account for the majority of variation (Härdle & Simar, 2015b). Discriminant analysis, on the other hand, aims to classify new observations (i.e., SAM

data) into groups known a priori (i.e., laboratory sulfides and sulfates). QDA, as an extension of linear discriminant analysis, does not assume equal covariance matrices between known classifications and identifies classification regions with quadratic, rather than linear, functions (Härdle & Simar, 2015a). While discriminant analyses assume multivariate normal distributions of the data, a benefit of QDA is that it is robust to violations of the assumption of normality (as is the case for the EGA data here) and often outperforms other classification techniques (Finch & Schneider, 2006).

QDA is a standard method for classifying unknown data based on a training data set and has found use in a range of disciplines including finance (Altman & Loris, 1976), molecular biology (Zhang, 1997), and geochemistry (Wang et al., 2018). Here, SO<sub>2</sub>, CO<sub>2</sub>, COS, CS<sub>2</sub>, and BSW areas from the laboratory EGA experiments were used as training data. Each sample had an assigned “sulfide” or “no sulfide” label. Based on the relationships between the variables and their labels, the QDA clusters the samples in the five-dimensional space and demarcates a region separating sulfides from sulfates. The same variables are used for the Mars samples, which do not have associated labels and are considered the “unknowns.” Based on the values of the five variables and the training data, the QDA predicts whether an unknown sample clusters with the sulfides or sulfates. Posterior probabilities for the Mars samples are calculated to report the likelihood that the prediction is correct compared to the training data. QDA was performed in Python 2.7.14. Statistics and figures were completed with scikit-learn (Pedregosa et al., 2011), Pandas (McKinney, 2010), NumPy (van der Walt et al., 2011), SciPy (Virtanen et al., 2019), and Matplotlib (Hunter, 2007).

### 3.3. Normalization Methods and Zero Removal

The calculated areas independently underwent various types of normalization. Four different processing methods were used to determine the data set that most accurately differentiated between sulfide- and nonsulfide-containing laboratory samples. These methods were (1) raw calculated areas, (2) log-transformed areas ( $\log_{10}[\text{counts}+1]$ ), (3) normalized to total sample mass and log-transformed, and (4) normalized to calculated SO<sub>2</sub> evolved from 75°C–600°C and log-transformed. For the final analysis used here, nondetections and zero values of COS and CS<sub>2</sub> were not included because they do not accurately reflect SAM data and introduce an artificial source of bias in the QDA where all samples with COS and CS<sub>2</sub> are classified as containing sulfide.

We did not normalize to estimated sulfur masses from either the Alpha Particle X-Ray Spectrometer (APXS) or SAM for several reasons. APXS reports the total amount of sulfur within its analysis area. The amount of sulfur observed by APXS is typically higher than that observed by SAM (Knudson et al., 2018). This difference is due to in large part to the ubiquity of CaSO<sub>4</sub> on Mars, which is measured in APXS analyses, but is not observed by SAM because it evolves sulfur volatiles above the temperature range used by SAM. Normalizing to this larger total sulfur value in Mars samples would artificially decrease the normalized amount of SO<sub>2</sub> evolved by SAM. Similarly, we chose not to normalize by estimated sulfur from SAM measurements because estimated sulfur is derived from evolved major SO<sub>2</sub> peaks. The calculation often includes SO<sub>2</sub> evolved at temperatures above the <600°C used for analysis in this work, due to the presence of Fe- and/or Mg-sulfates, which overestimates the relevant sulfur. It also propagates a second source of error—the mass of sample delivered to SAM and total weight percent of sulfur. These calculations also exclude reduced sulfur volatile (e.g., H<sub>2</sub>S, COS, and CS<sub>2</sub>) contributions to the weight percent estimates.

### 3.4. Area Under Curve-Receiver Operating Characteristics

To test which set of training data most accurately predicted samples with sulfides or sulfates, we used area under curve-receiver operating characteristics (AUC-ROC). This metric compares the true positive rate to the false positive rate at different thresholds for classification (e.g., determines true positive rate if using a 90% probability that classification is correct versus 50% probability) during a QDA of training data. These rates can be plotted against each other and an AUC score can be calculated, with an AUC score between zero and one. An AUC score of one is an ideal scenario and means the discrimination method correctly groups samples every time. An AUC score of one-half means the method is no different from random guessing. An AUC score of zero means the method incorrectly predicts groups for every sample.

Using the AUC-ROC metric for the different data processing methods, we chose the log-transformed training data set that normalized samples to the total mass. The AUC score for this training data was 0.98, which

suggests a high degree of accuracy in discriminating between sulfides and sulfates. The AUC score for unnormalized training data was also 0.98; however, this similarity in AUC score was likely due to similarity in total sample sizes of the laboratory data (between 5 and 10 mg). For a more accurate comparison to the Mars data, we chose the normalized masses because Mars sample masses ranged from ~20 to 135 mg. Training data sets without log transformation and normalized to low-temperature SO<sub>2</sub> evolution had AUC scores of 0.71 and 0.40, respectively.

### 3.5. Spearman Correlation Coefficient Analysis

Spearman rank-order correlation coefficients ( $\rho$ ) and two-tailed  $p$ -values were calculated between all pairs of volatiles' areas after mass normalization. Data were grouped by laboratory sulfides ( $N = 34$ ), laboratory sulfates ( $N = 22$ ), Mars samples in which QDA identified sulfides ( $N = 10$ ), and Mars samples in which sulfides were not detected (SND) by QDA ( $N = 14$ ). Potentially significant differences between these data subsets' pairs of volatiles' correlations were identified through the following steps. First, Spearman correlation coefficients were transformed to  $z$ -values by the Fisher's  $Z$ -transformation to ensure a normal distribution. The  $z$ -values were then compared to determine a “ $Z$ -observed” by the following formula (Myers & Sirois, 2006):

$$Z_{\text{obs}} = \frac{z_1 - z_2}{\sqrt{\frac{1}{N_1 - 3} + \frac{1}{N_2 - 3}}}$$

Using a normal distribution, the  $Z_{\text{obs}}$  was compared to critical values to determine two-tailed  $p$ -values to identify potentially significant differences. All calculations were performed using Python SciPy and Microsoft Excel.

## 4. Results and Discussion

### 4.1. EGA Comparisons

The EGA profiles of the five variables used in the QDA were produced for eight Martian samples: John Klein 4 (JK, fourth sample of JK), Cumberland 3 (CB, third sample of CB), Oudam (OU), Big Sky (BS), Duluth (DU), Stoer (ST), Highfield (HF), and Rock Hall (RH). JK, CB, and OU are mudstones (JK and CB are samples of the Sheepbed mudstone, and OU is a sample of the Murray mudstone) that had previous evidence from CheMin and/or SAM isotopes suggesting the presence of reduced sulfur (Franz et al., 2017; Vaniman et al., 2014). BS is a sample of the Stimson sandstone that appears to contain sulfide based on the QDA (section 4.3). DU is another Murray Formation mudstone that lies stratigraphically just below VRR. The three remaining samples (ST, HF, and RH) are from two members of VRR (ST is a sample from the Pettegrove Point member, HF and RH are gray and red samples of the Jura member, respectively) and were plotted for comparison. See Figure S1 for additional stratigraphic context. These profiles are shown in Figures 1a–1e. Profiles were adjusted to show normalized sample sizes of 45 mg with the assumption that larger or smaller samples were homogeneous. Each volatile uses the same scale across samples. These profiles were produced from original data and may differ from previously reported EGA curves due to differences in background subtraction, smoothing, and refinements in the temperature model (section 3.1). The EGA profiles presented here focus on traces used in the QDA and to show examples that, based on the evolution of different volatiles, may (or may not) be indicative of sulfide.

Figure 1a shows the profiles of SO<sub>2</sub> for the eight Martian samples. All profiles of SO<sub>2</sub>, except for HF, begin to increase dramatically between 350°C and 550°C. These are the beginnings of the main SO<sub>2</sub> peaks that can be attributed to iron sulfates or iron sulfides. Notably, however, there are small peaks of SO<sub>2</sub> (or corrected  $m/z$  66) in all samples except JK at temperatures below the beginning of the main peak. These small, low temperature peaks could be the result of sulfide or elemental sulfur oxidation (McAdam et al., 2020) or, alternatively, sulfonic acids (Franz et al., 2017). These low temperature evolutions of SO<sub>2</sub> are consistent with SO<sub>2</sub> observed during EGA of troilite in the laboratory. RH and HF have among the largest and longest evolutions of SO<sub>2</sub> in this lowest temperature range, possibly hinting at the presence of reduced sulfur in these samples. Importantly, ST and DU also have low temperature peaks (<200°C), but these correlate with BSW (Figure 1e), suggesting the presence of MTBSTFA that could be contributing interfering masses.

Figures 1b and 1c show the COS and CS<sub>2</sub> profiles of the Martian samples. Interestingly, RH and HF have the most complicated structures of COS and CS<sub>2</sub> with several peaks spanning hundreds of degrees Celsius. The

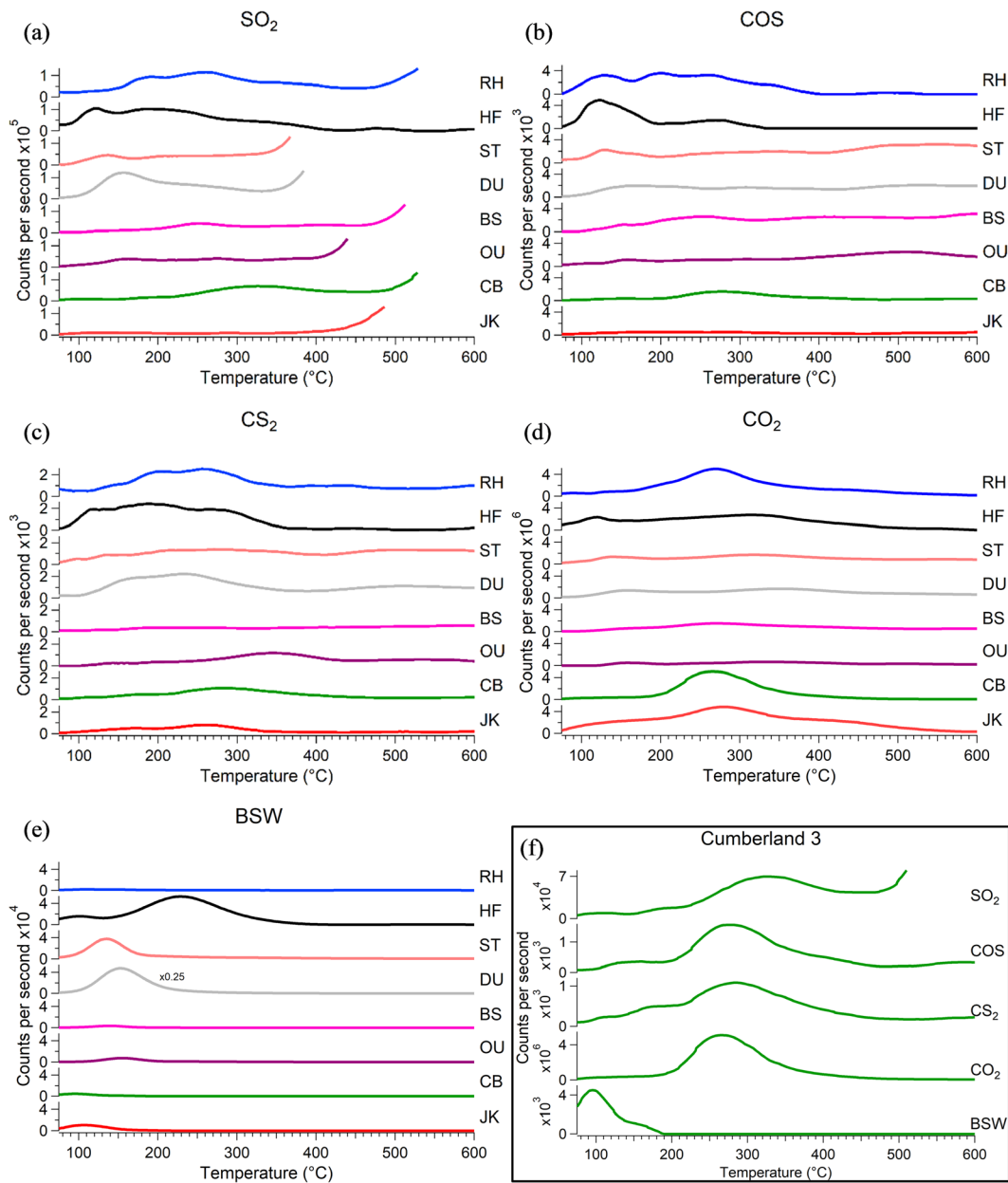


**Figure 1.** (a–e) EGA profiles of  $\text{SO}_2$  ( $m/z$  66),  $\text{COS}$  ( $m/z$  60),  $\text{CS}_2$  ( $m/z$  76),  $\text{CO}_2$  ( $m/z$  45), and  $\text{BSW}$  ( $m/z$  147) for select Martian drilled samples. Each profile has been vertically adjusted to represent the relative intensities of the volatile evolutions from a theoretical 45 mg homogeneous sample. Each volatile has the same y-axis scale across samples. The  $\text{BSW}$  profile for  $\text{DU}$  has been vertically reduced by a factor of four to fit on the same scale as the other samples. Horizontal axes all range from 75°C to 600°C, the range used for area calculations. The  $\text{SO}_2$  plots focus on the low temperature volatile evolution; the starting tails of the main  $\text{SO}_2$  peaks in the samples are seen as inflection points. (f) EGA profiles from  $\text{CB}$  as an example of the volatiles' (co-)evolutions. Each profile's vertical axis in this plot has been adjusted to emphasize profile structure.

$\text{COS}$  peaks in  $\text{ST}$  and  $\text{DU}$  largely correspond with the evolution of  $\text{BSW}$ , suggesting the possibility of interfering masses from  $\text{MTBSTFA}$  and/or its byproducts.  $\text{BS}$  has a  $\text{COS}$  peak around 250°C, but relatively little  $\text{CS}_2$  structure.  $\text{OU}$  has two small peaks of  $\text{COS}$  (~150°C and 500°C) and one peak of  $\text{CS}_2$  (350°C).  $\text{JK}$  and  $\text{CB}$  each have two shallow peaks of  $\text{CS}_2$  below ~300°C.  $\text{CB}$  has a clear  $\text{COS}$  peak, while  $\text{JK}$  offers little in terms of structure beyond a broad, shallow evolution, though their integrated counts are similar.

Figure 1d shows  $\text{CO}_2$  evolution in the select Martian samples. Interestingly,  $\text{OU}$ ,  $\text{DU}$ ,  $\text{ST}$ , and  $\text{HF}$  have broadly similar  $\text{CO}_2$  evolutions with a shallow peak between 100°C and 200°C and another around 350°C. The lower temperature peaks of  $\text{CO}_2$  in these four Martian samples do correspond to peaks of  $\text{SO}_2$ ,  $\text{COS}$ ,



and CS<sub>2</sub>. The CO<sub>2</sub> also corresponds with BSW in OU, DU, and ST, but not HF. The coevolution of the five volatiles in these three samples may suggest that the reduced sulfur volatile discriminants are a result of interactions with MTBSTFA. The lack of correlation with BSW in HF could be indicative of reactions between a reduced sulfur component and CO or CO<sub>2</sub>. JK, CB, and RH, on the other hand, have single, larger peaks of CO<sub>2</sub> between 250°C and 300°C. However, with the exception of CO<sub>2</sub> and CS<sub>2</sub> in JK, the CO<sub>2</sub> does not clearly correspond to any other volatile evolutions.

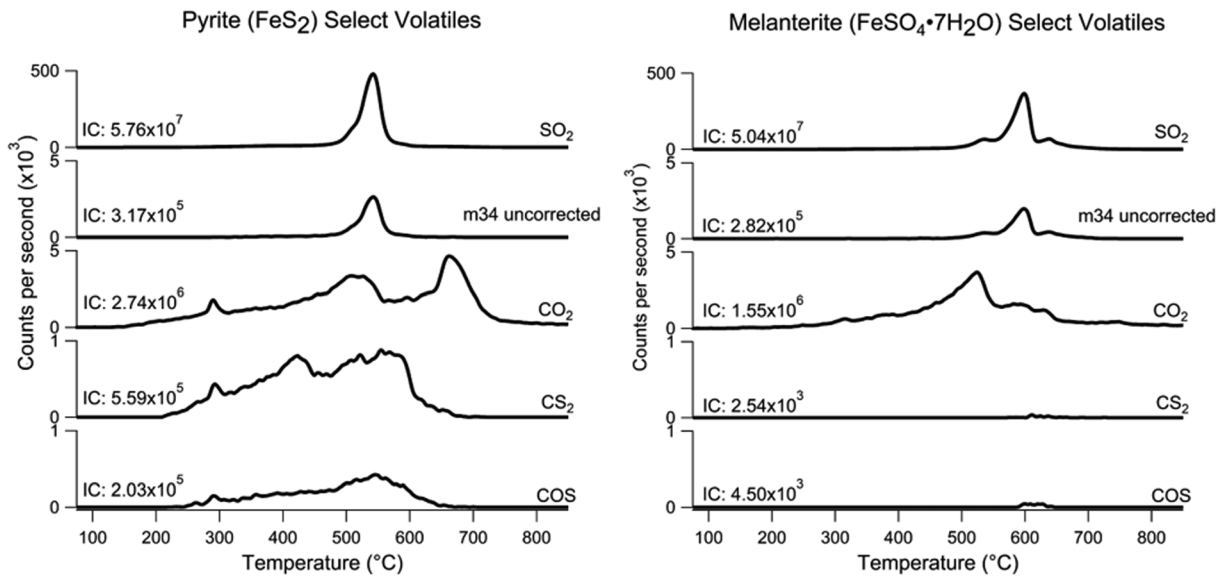
Figure 1e shows the BSW in the eight Martian samples. All Martian samples have some BSW due to the presence of MTBSTFA vapor in the SMS, which reacts with water (Freissinet et al., 2019). However, some samples produce more BSW than others and the differences are likely a function of how much MTBSTFA and water were present. The amount of MTBSTFA vapor present for reactions is variable and affected by factors such as how long a cup has been exposed to the SAM SMS, whether a sample had previously been used in the cup, the number of pyrolysis runs since the full-cup wet chemistry experiment was run (Millan et al., 2019), and the amount of powder in the cup, which acts as a matrix for adsorption of the MTBSTFA vapor from the instrument background. Of the samples shown in Figure 1e, DU has 3–5 times as much evolved BSW as HF and ST. The other samples have relatively small peaks of BSW that occur below 200°C.

Figure 1f shows a reconsolidated plot of all five volatiles for a single sample: Cumberland 3, which has the strongest case for presence of a reduced sulfur compound. The vertical axes in this panel have been optimized to emphasize the profile structures and demonstrate coevolutions of volatiles. The SO<sub>2</sub> peak around 300°C is consistent with the oxidation of a sulfide or elemental sulfur. At approximately the same temperature as the SO<sub>2</sub> evolution, COS, CS<sub>2</sub>, and CO<sub>2</sub> coevolve. The coevolution of these four volatiles is indicative of a reaction or decomposition. It is possible that a reduced sulfur compound is reacting with the CO<sub>2</sub> or CO to form COS and CS<sub>2</sub>. It is also possible that the approximate coevolution is the result of the breakdown of a sulfur-containing organic. Relatively little BSW is evolved and its evolution is not correlated with other volatiles used in the analysis. Taken together, the BSW result in CB suggests that MTBSTFA is not a likely complicating factor in the production of the COS and CS<sub>2</sub>, prime potential indicators of reduced sulfur.

Similar to CB, RH has relatively little BSW that mostly evolved at low temperature. RH also has coevolving peaks of CO<sub>2</sub>, SO<sub>2</sub>, CS<sub>2</sub>, and COS between 350°C and 400°C. RH has additional COS and CS<sub>2</sub> peak evolutions below 350°C that are not clearly correlated with CO<sub>2</sub> or BSW. DU and ST are unlike CB and RH in terms of these five volatiles. While CO<sub>2</sub>, SO<sub>2</sub>, CS<sub>2</sub>, and COS have coevolving peaks around 150°C, they are accompanied by a large peak of BSW in both DU and ST. The coevolution of BSW, as an MTBSTFA indicator, with the other four volatiles suggests that MTBSTFA, its byproducts, and their fragments are related to these peaks. Interestingly, OU has similar behavior to DU and ST in terms of BSW and the other volatiles with coevolving peaks around 150°C, though the peak of BSW is much smaller in OU than DU or ST. HF is different from all of these samples in that its main peak of BSW evolves above 200°C and does not clearly coevolve with the other peaks. However, around 120°C, there are coevolving peaks similar to CB. BS has coevolving peaks of SO<sub>2</sub>, COS, and CO<sub>2</sub> around 250°C, while BSW and CS<sub>2</sub> evolve shallow peaks at lower temperatures. JK has little structure of SO<sub>2</sub> and COS below 400°C, but its CS<sub>2</sub> and CO<sub>2</sub> peaks approximately coevolve, and it has only a small peak of BSW that evolved before the other volatiles. The volatile comparison profiles for each of these samples can be found in Figure S2.

#### 4.2. Laboratory EGA Results

The various laboratory samples and mixtures were analyzed by EGA and example iron sulfide (pyrite) and iron sulfate (melanterite) volatile products are shown in Figure 2. These two sulfur compounds were chosen to demonstrate their similarities and differences in key volatile evolutions. Both compounds evolved SO<sub>2</sub> around the same temperature (550°C – 600°C). SO<sub>2</sub> from sulfates results from sulfate decomposition. Sulfides alone, counterintuitively, consistently evolve SO<sub>2</sub> in EGA experiments (McAdam et al., 2014; Stern et al., 2013) with minor O<sub>2</sub> or H<sub>2</sub>O likely serving as oxidants. The decomposition of other compounds, such as oxychlorines, can also provide oxygen for sulfide oxidation. While sulfides can evolve elemental/molecular sulfur ions (i.e., S<sub>n</sub><sup>+</sup>; *m/z* 32, 64, 96, 128, 160, 192, 224, 256), the mass spectra of the evolved gases are not consistent with major S<sub>n</sub><sup>+</sup> evolution during our experiments (Table S1). Additionally, *m/z* 48 (SO) is a major fragment that tracks *m/z* 64, which is consistent with SO<sub>2</sub> rather than S<sub>2</sub> evolution.



**Figure 2.** Comparison of laboratory EGA results for pyrite ( $\text{FeS}_2$ , left) and melanterite ( $\text{FeSO}_4 \cdot 7\text{H}_2\text{O}$ , right). Each mineral was mixed in a 9:1 ratio of fused silica to S-mineral by mass. From top to bottom, EGA evolutions of  $\text{SO}_2$  ( $m/z$  64), m34 uncorrected (overwhelmingly  $\text{SO}_2$  fragments, unlikely  $\text{H}_2\text{S}$ ),  $\text{CO}_2$  ( $m/z$  44),  $\text{CS}_2$  ( $m/z$  76), and  $\text{COS}$  ( $m/z$  60). IC = integrated counts for each mass from  $75^\circ\text{C}$  to  $850^\circ\text{C}$ . Additional example plots are in the (Figure S3).

Given the similarity in temperature release and amount of  $\text{SO}_2$  evolved, Figure 2 highlights the difficulty in using  $\text{SO}_2$  as a sole indicator of sulfide versus sulfate presence. Evolved  $\text{H}_2\text{S}$  could be used as a sulfide indicator due to its possible production through reactions between sulfides and  $\text{H}_2$ ,  $\text{HCl}$ , or  $\text{H}_2\text{O}$ . However,  $\text{H}_2\text{S}$  can also form from oven reactions between  $\text{SO}_2$  and  $\text{H}_2$  (McAdam et al., 2014). The  $\text{H}_2\text{S}$  mass-to-charge ratio ( $m/z$  34) is also not necessarily diagnostic of  $\text{H}_2\text{S}$ ; rather, it can be the result of isotopically heavy oxygen ( $^{16}\text{O}^{18}\text{O}$ ) or  $^{34}\text{S}$ , either of which could come from fragments of  $\text{SO}_2$ . Given these interferences, the laboratory EGA experiments did not produce an appreciable amount of  $\text{H}_2\text{S}$  ( $m/z$  34) from sulfides or sulfates, regardless of mixtures. The observed  $m/z$  34 tracks with  $\text{SO}_2$  from sulfides and sulfates and is interpreted as a fragment of  $\text{SO}_2$  (Figure 2). The lack of production of  $\text{H}_2\text{S}$  in the laboratory is likely from water background and oxygen leaks in laboratory systems, which are greater on Earth than on Mars and can result in oxidation to  $\text{SO}_2$ . Similar experiments were performed using a laboratory GC-MS setup and again showed that evolved  $\text{H}_2\text{S}$  is not a strong discriminator between sulfides and sulfates (Figure S4).

We also investigated the evolution of carbon (as  $\text{CO}_2$ ) given its role in the production of carbon-sulfur volatiles (Figure 2). Sources for  $\text{CO}_2$  include: the background in the EGA data, as an oxidation product of organics, and/or from decomposition of carbonates. In Figure 2,  $\text{CO}_2$  evolves in similar amounts over a range of temperatures in both melanterite and pyrite. A search for organic fragments (e.g.,  $m/z$  55, 58, and 78, indicative of alkyl groups, acetone, and benzene, respectively) in the EGA runs did not indicate the type of carbon compounds that may have been present—most carbon appears to have been oxidized. Importantly, all samples and mixtures evolved  $\text{CO}_2$  in variable amounts. While the integrated counts of  $\text{CO}_2$  spanned several orders of magnitude for laboratory samples used in the QDA ( $\sim 3.3 \times 10^4$  to  $\sim 2.8 \times 10^7$ ), there were no statistically significant ( $p < 0.05$ ) differences in counts of  $\text{CO}_2$  across different sulfur minerals. Additionally, all samples that evolved greater than  $10^6$  integrated counts of  $\text{CO}_2$  in the laboratory EGA were intentional mixtures with carbon-containing compounds (Figure S5). Based on these observations, we conclude that any organic contaminants in the laboratory EGA to be at trace levels.

Despite similarities in profiles and amounts of  $\text{SO}_2$ ,  $m/z$  34, and  $\text{CO}_2$ , significant differences in evolution of  $\text{COS}$  and  $\text{CS}_2$  were observed in sulfides versus sulfates. Figure 2 demonstrates this difference with both  $\text{COS}$  and  $\text{CS}_2$  having evolved approximately two orders of magnitude greater integrated count areas in pyrite compared to melanterite. Both pyrite and troilite (Figure S3) evolved more  $\text{COS}$  and  $\text{CS}_2$  than any of the sulfates when tested alone, without being mixed with additional volatile-evolving compounds. Troilite typically

**Table 2**  
QDA Results for 24 Martian EGA Samples

| Mars sample            | QDA classification (i.e., "Did this sample cluster with the lab sulfides?") | Probability of the Mars sample clustering with the lab sulfides |
|------------------------|---|---|
| Rocknest 1 (RN1)       | No  | 10%   |
| Rocknest 2 (RN2)       | No  | 3%  |
| Rocknest 3 (RN3)       | No  | 1%  |
| Rocknest 4 (RN4)       | No  | 3%  |
| John Klein (JK)        | Yes   | 52%   |
| Cumberland (CB)        | Yes   | 89%   |
| Windjana (WJ)          | No  | 7%  |
| Confidence Hills (CH)  | No  | <1%   |
| Mojave (MJ)            | No  | <1%   |
| Telegraph Peak (TP)    | No  | <1%   |
| Buckskin (BK)          | No  | 1%  |
| Big Sky (BS)           | Yes   | 78%   |
| Greenhorn 1 (GH1)      | No  | <1%   |
| Greenhorn 2 (GH2)      | Yes   | 60%   |
| Gobabeb 1 (GB1)        | Yes   | 86%   |
| Gobabeb 2 (GB2)        | Yes   | 57%   |
| Oudam (OU)             | No  | 16%   |
| Marimba (MB)           | Yes   | 74%   |
| Ogunquit Beach 3 (OG3) | Yes   | 51%   |
| Quela (QL)             | No  | 1%  |
| Duluth (DU)            | No  | 1%  |
| Stoer (ST)             | No  | 3%  |
| Highfield (HF)         | Yes   | 95%   |
| Rock Hall (RH)         | Yes   | 95%   |

Note. Samples were considered to classify with the sulfides if the posterior probably was >50%.

evolved less COS and CS<sub>2</sub> than pyrite, which is consistent with troilite's relatively greater stability. The smallest difference in COS and CS<sub>2</sub> evolved for minerals on their own was CS<sub>2</sub> evolving about twice as much in troilite as in kieserite. This was an anomalous case, however, and troilite more typically evolved 1 and 2 orders of magnitude more COS and CS<sub>2</sub> than any of the sulfates. Pyrite evolved even more COS and CS<sub>2</sub>: usually 2 and 3 orders of magnitude more than the sulfates. These trends held for most mixtures, too, where *m/z* 60 and 76 productions were typically 1–3 orders of magnitude greater with the sulfides compared to the sulfates.

Notable exceptions to the trends in COS and CS<sub>2</sub> described above occurred during EGA of mixtures with high levels of added carbon, such as Mg-acetate, myristic acid, and MTBSTFA-DMF. The elevated production of COS and CS<sub>2</sub> were likely due to the large amounts of reduced carbon in those samples and interfering mass fragments of these larger molecules or their byproducts. It was expected that the addition of large amounts of organic matter would increase the evolved COS and CS<sub>2</sub> of both sulfates and sulfides due to both the increased reducing power available and increased carbon. However, in samples without added carbon sources, sulfides still typically evolved orders of magnitude more COS and CS<sub>2</sub>, possibly through direct reactions with evolved CO<sub>2</sub>. While such reactions may be slow at temperatures <600°C, they have, nonetheless, been observed in other works (Shao et al., 1994; B. Wang et al., 2014). It should also be noted that evolved COS and CS<sub>2</sub> are minor components of the total evolved sulfur gases (e.g., SO<sub>2</sub> counts are up to five orders of magnitude greater than COS and CS<sub>2</sub> counts in laboratory analyses). Based on the carbon-containing EGA mixtures, it was estimated that several millimoles of added carbon per mg sample would be required for sulfates to consistently produce comparable levels of COS and CS<sub>2</sub> as sulfides (Figure S5). This would represent much more carbon than is typically observed in EGA by SAM, which, based on CO<sub>2</sub>, has been reported at levels of at most 2,373 ± 820 μgC(CO<sub>2</sub>)/g (~0.10 ± 0.04 mmol/mg; Sutter et al., 2017).

### 4.3. QDA Results

Based on the data processing described in sections 3.2 and 3.3, we used a training data set with 56 samples that included sulfides and sulfates in different mixtures (section 2.3). From this training data set, we

performed a randomized QDA validation test. For this validation, half of the training data sets ( $N = 28$ ) were randomly selected for the QDA fit. Predictions were performed on the other half of the training data. The AUC-ROC score for this data validation and the percentage of correct classifications of the predictions were calculated. The validation was repeated 50 times. From the 50 randomly selected training data sets, samples were correctly classified (i.e.,  $>50\%$  posterior probability) an average of 77.93% (standard deviation of 9.00%) of the time (see Figure S6), which is comparable to previous work using QDA (Wang et al., 2018). The average AUC score for the 50 validation runs was 0.99 (standard deviation of 0.01), which indicates a high level of discriminating power within this training data set.

When predictions with the training data were made, several samples stood out as clustering with the sulfide training data ( $>50\%$  calculated posterior probability of clustering with the sulfide training data). Table 2 lists all of the Martian samples analyzed, whether they classified with the sulfides, and their calculated posterior probabilities. Among the samples that were identified as containing reduced sulfur were JK, CB, BS, HF, and RH. Previous work has indicated that JK and CB contain small amounts of pyrrhotite and possibly pyrite (Vaniman et al., 2014), described further in section 4.5.2. HF and RH are two samples that were collected from the Jura member of VRR. Interestingly, DU and ST, which are samples collected from the Blunts Point and Pettegrove Point members of the near-VRR and VRR, respectively, were not identified in the QDA as likely to contain reduced sulfur. The training data and Mars samples are plotted in Figure 3. This figure shows the clustering of select Martian samples that were identified as containing sulfides compared to those that were not. While DU, ST, HF, and RH all evolved similar amounts (within an order of magnitude after sample size normalization) of  $\text{CO}_2$ , COS, and  $\text{CS}_2$ , HF and RH evolved approximately 10 times less  $\text{SO}_2$  than the other two samples. BSW was variable across the four samples, with DU having the highest and RH having the lowest integrated counts. Taken together, this information suggests that evolved  $\text{SO}_2$  is an important discriminating factor in the QDA in which less evolved  $\text{SO}_2$  is consistent with reduced sulfur, which is logical in an inert/poorly oxidizing environment.

#### 4.4. Spearman Correlation Coefficient Results

The Spearman's  $\rho$  between pairs of volatiles can provide insight into both the reactions that may have occurred during volatile coevolution and the differences between subsets of the data. Figure 4 shows both the Spearman correlation coefficients for four subsets of the data as well as differences between data subsets with potential significance marked in bold.

##### 4.4.1. Laboratory Results

The laboratory sulfides show significant correlations between  $\text{SO}_2$  and COS ( $\rho = 0.40$ ,  $p < 0.05$ ),  $\text{SO}_2$  and  $\text{CS}_2$  ( $\rho = 0.56$ ,  $p < 0.01$ ), and COS and  $\text{CS}_2$  ( $\rho = 0.79$ ,  $p < 0.01$ ). The sulfides appear to have a weak positive correlation between  $\text{CO}_2$  and COS ( $\rho = 0.31$ ,  $p < 0.1$ ).

The laboratory sulfates are similar to the sulfides in that they show significant correlations between  $\text{SO}_2$  and COS ( $\rho = 0.65$ ,  $p < 0.01$ ),  $\text{SO}_2$  and  $\text{CS}_2$  ( $\rho = 0.69$ ,  $p < 0.01$ ), and COS and  $\text{CS}_2$  ( $\rho = 0.79$ ,  $p < 0.01$ ). Also similar are the weaker correlations between  $\text{CO}_2$  and COS ( $\rho = 0.40$ ,  $p < 0.1$ ) and  $\text{CO}_2$  and  $\text{CS}_2$  ( $\rho = 0.40$ ,  $p < 0.1$ ). A key difference between the data subsets, however, is the significant correlation between  $\text{SO}_2$  and  $\text{CO}_2$  ( $\rho = 0.67$ ,  $p < 0.01$ ).

This difference is reflected in the bottom table and demonstrates that the laboratory sulfides have a significantly lower Spearman's rho than the laboratory sulfates for the  $\text{SO}_2$  vs.  $\text{CO}_2$  comparison ( $\rho_{\text{difference}} = -0.64$ ,  $p < 0.01$ ). The difference in correlation coefficients for  $\text{CO}_2$  and  $\text{CS}_2$  ( $\rho_{\text{difference}} = -0.49$ ,  $p < 0.1$ ) also tends toward significance. No other significant differences in Spearman's rho were observed. The positive correlation between  $\text{SO}_2$  and  $\text{CO}_2$  in the laboratory sulfates appears to be largely driven by the sulfate samples that had added reduced carbon (MTBSTFA, acetate, myristic acid). There appears to be a moderate increase in evolved  $\text{SO}_2$  when reduced carbon is added to the samples; though the effect seems to be mineral-dependent where melanterite was more affected than jarosite and the sulfates were more affected than the sulfides. Plots of the data are presented in the Figure S8.

##### 4.4.2. Mars Results

The Mars samples that contain reduced sulfur according to the QDA have few significant correlations between variables. COS and  $\text{CS}_2$  are strongly correlated ( $\rho = 0.68$ ,  $p < 0.05$ ) while  $\text{SO}_2$  and  $\text{CO}_2$  appear more moderately positively correlated ( $\rho = 0.61$ ,  $p < 0.1$ ). No significant correlations were observed between BSW



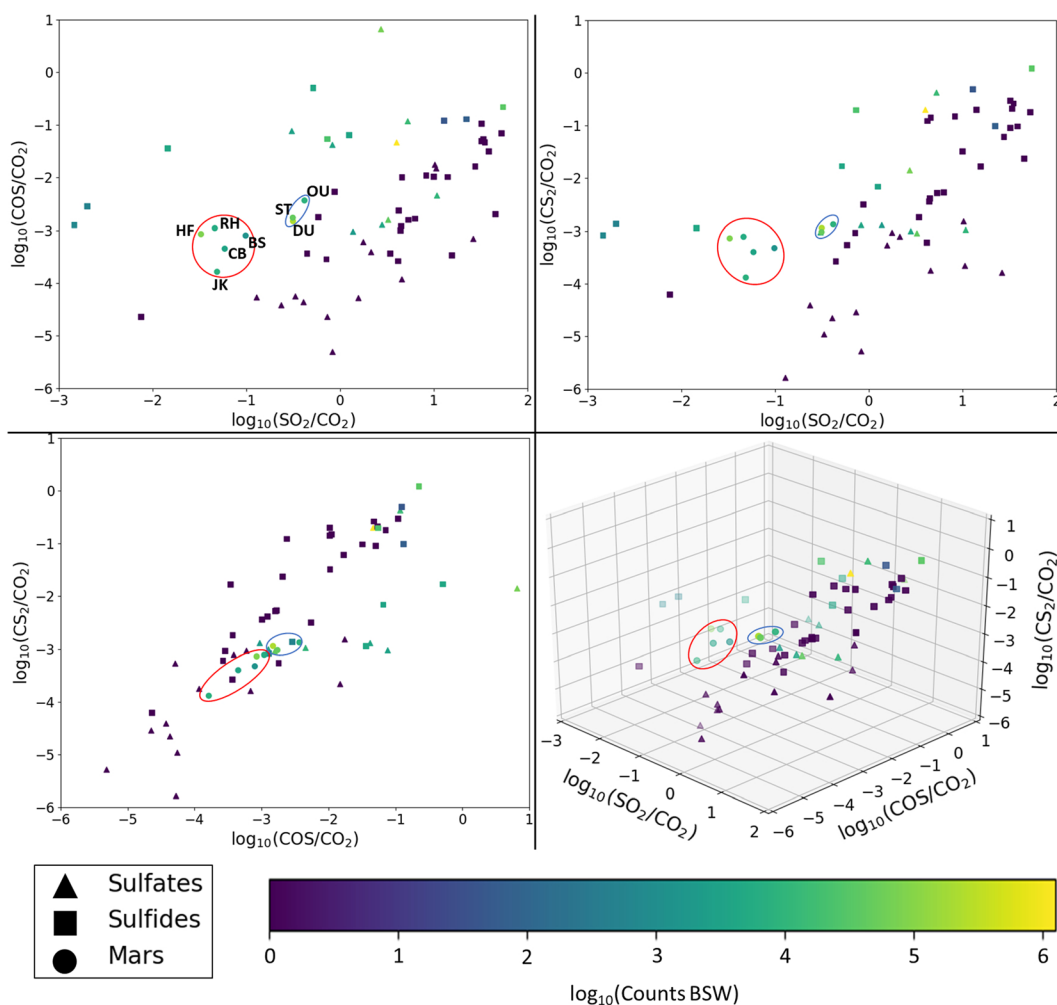


**Figure 3.** This figure shows 2-D and 3-D plotting of the volatiles for the training data and eight select Martian samples. The 2-D plots show face-on views of the 3-D plot from different perspectives. Counts of  $\text{SO}_2$ ,  $\text{CS}_2$ , and  $\text{COS}$  have been divided by counts of  $\text{CO}_2$  and are shown in the plot as the  $\log_{10}$  of these ratios. The  $\log_{10}$  of the BSW counts are shown according to the color bar. The ellipses mark out which Martian samples clustered with the laboratory sulfides (red) and which did not (blue) according to the QDA. The ellipses are illustrative only. Refer to Figure S7 for zoomed-in versions of the 2-D plots.

and any of the other volatiles. Importantly, it should be noted that these samples were identified in the QDA as likely to contain reduced sulfur, but these samples largely contain sulfate.

The Mars SND samples have three important correlations.  $\text{COS}$  and  $\text{CS}_2$  are again strongly positively correlated ( $\rho = 0.85$ ,  $p < 0.01$ ).  $\text{CS}_2$  and BSW are strongly positively correlated ( $\rho = 0.73$ ,  $p < 0.01$ ) while  $\text{COS}$  and BSW are similarly correlated to a lesser extent ( $\rho = 0.51$ ,  $p < 0.1$ ). Given the interferences MTBSTFA can produce, these correlations suggest that MTBSTFA/BSW may affect the observed  $m/z$  60 and 76 ( $\text{COS}$  and  $\text{CS}_2$ ) in the Mars SND samples. The other two marked correlations— $\text{CO}_2$  and  $\text{COS}$  ( $\rho = -0.56$ ,  $p < 0.05$ ) and  $\text{SO}_2$  and  $\text{CS}_2$  ( $\rho = 0.49$ ,  $p < 0.1$ )—are driven by a sampling effect from the four Rocknest samples (see Figure S8). These correlations go away when only a single representative Rocknest sample (RN3) is used in the correlation analysis.

The differences in Spearman's rho between the two Martian data subsets are reflected in the third table.  $\text{SO}_2$  and  $\text{CO}_2$  have a stronger correlation ( $\rho_{\text{difference}} = 0.78$ ,  $p < 0.1$ ) in the samples with reduced sulfur as identified by QDA.  $\text{CO}_2$  and  $\text{COS}$  have a significantly different correlation in the two subsets ( $\rho_{\text{difference}} = 0.89$ ,  $p < 0.05$ ): Mars SND had a negative correlation, while Mars QDA sulfides had a weak, nonsignificant positive correlation. While it is tempting to interpret these correlations on Mars as being the result of sulfides or organic sulfur, the  $\text{SO}_2$  is likely driven largely by sulfate decomposition, which makes the interpretation

| Lab Sulfide (N=34) |                 |                 |               |                 |                  |
|--------------------|-----------------|-----------------|---------------|-----------------|------------------|
|                    | SO <sub>2</sub> | CO <sub>2</sub> | COS           | CS <sub>2</sub> | BSW <sup>‡</sup> |
| SO <sub>2</sub>    |                 | 0.03            | <b>0.40**</b> | <b>0.56***</b>  | 0.10             |
| CO <sub>2</sub>    |                 |                 | <b>0.31*</b>  | -0.09           | 0.27             |
| COS                |                 |                 |               | <b>0.79***</b>  | 0.47             |
| CS <sub>2</sub>    |                 |                 |               |                 | 0.43             |
| BSW                |                 |                 |               |                 |                  |

| Lab Sulfate (N=22) |                 |                 |                |                 |                  |
|--------------------|-----------------|-----------------|----------------|-----------------|------------------|
|                    | SO <sub>2</sub> | CO <sub>2</sub> | COS            | CS <sub>2</sub> | BSW <sup>‡</sup> |
| SO <sub>2</sub>    |                 | <b>0.67***</b>  | <b>0.65***</b> | <b>0.69***</b>  | 0.15             |
| CO <sub>2</sub>    |                 |                 | <b>0.40*</b>   | <b>0.40*</b>    | -0.50            |
| COS                |                 |                 |                | <b>0.79***</b>  | 0.25             |
| CS <sub>2</sub>    |                 |                 |                |                 | 0.57             |
| BSW                |                 |                 |                |                 |                  |

| Lab Sulfide vs. Lab Sulfate ( $\rho_{\text{difference}}^{\dagger}$ ) |                 |                 |       |                 |       |
|--|-----------------|-----------------|-------|-----------------|-------|
|  | SO <sub>2</sub> | CO <sub>2</sub> | COS   | CS <sub>2</sub> | BSW   |
| SO <sub>2</sub>  |                 | <b>-0.64***</b> | -0.25 | -0.13           | -0.05 |
| CO <sub>2</sub>  |                 |                 | -0.09 | <b>-0.49*</b>   | 0.77  |
| COS  |                 |                 |       | 0.00            | 0.22  |
| CS <sub>2</sub>  |                 |                 |       |                 | -0.14 |
| BSW  |                 |                 |       |                 |       |

| Mars QDA Sulfide (N=10) |                 |                 |      |                 |       |
|-------------------------|-----------------|-----------------|------|-----------------|-------|
|                         | SO <sub>2</sub> | CO <sub>2</sub> | COS  | CS <sub>2</sub> | BSW   |
| SO <sub>2</sub>         |                 | <b>0.61*</b>    | 0.25 | -0.08           | -0.49 |
| CO <sub>2</sub>         |                 |                 | 0.32 | -0.12           | 0.24  |
| COS                     |                 |                 |      | <b>0.68**</b>   | 0.21  |
| CS <sub>2</sub>         |                 |                 |      |                 | 0.15  |
| BSW                     |                 |                 |      |                 |       |

| Mars SND (N=14) |                 |                 |                |                 |                |
|-----------------|-----------------|-----------------|----------------|-----------------|----------------|
|                 | SO <sub>2</sub> | CO <sub>2</sub> | COS            | CS <sub>2</sub> | BSW            |
| SO <sub>2</sub> |                 | -0.17           | 0.39           | <b>0.49*</b>    | -0.05          |
| CO <sub>2</sub> |                 |                 | <b>-0.56**</b> | -0.38           | -0.05          |
| COS             |                 |                 |                | <b>0.85***</b>  | <b>0.51*</b>   |
| CS <sub>2</sub> |                 |                 |                |                 | <b>0.73***</b> |
| BSW             |                 |                 |                |                 |                |

| Mars Sulfide vs. Mars SND ( $\rho_{\text{difference}}^{\dagger}$ ) |                 |                 |               |                 |       |
|--|-----------------|-----------------|---------------|-----------------|-------|
|  | SO <sub>2</sub> | CO <sub>2</sub> | COS           | CS <sub>2</sub> | BSW   |
| SO <sub>2</sub>  |                 | <b>0.78*</b>    | -0.14         | -0.57           | -0.44 |
| CO <sub>2</sub>  |                 |                 | <b>0.88**</b> | 0.26            | 0.29  |
| COS  |                 |                 |               | -0.17           | -0.30 |
| CS <sub>2</sub>  |                 |                 |               |                 | -0.58 |
| BSW  |                 |                 |               |                 |       |

**Figure 4.** These tables show the Spearman's rho correlation coefficients for subsets of the data (top four tables) and the differences in the rho values between the either lab or Mars data subsets (bottom two tables). The three tables on the left focus on laboratory data. The three tables on the right focus on Mars data with samples divided based on how they clustered in the QDA. Any correlation or difference in correlation with  $p < 0.1$  is bolded. Approximate  $p$ -values are represented with asterisks: \* $p < 0.1$ , \*\* $p < 0.05$ , \*\*\* $p < 0.01$ . <sup>†</sup>Significance of  $\rho_{\text{difference}}$  calculated by z-score comparison as described in section 3.5. <sup>‡</sup>Only samples with measured  $m/z$  147 were used in calculating these correlations,  $N = 9$  for each of the laboratory sulfides and laboratory sulfates.

difficult. No other significant differences in Spearman's rho were observed. The relatively few differences could be due to small sample size or the presence of sulfate in the samples that were identified as likely to contain sulfide by the QDA.

#### 4.5. Implications for Martian Samples and VRR

##### 4.5.1. Using COS and CS<sub>2</sub> as Key Proxy Indicators of Reduced Sulfur

This work provides the first case of using carbon sulfur gases observed in EGA to discriminate between mixed samples with reduced sulfur and those without. Previous work has looked at evolutions of COS and CS<sub>2</sub> as indicators of recalcitrant organosulfur compounds (Eigenbrode et al., 2018). Other EGA studies have also observed total COS and CS<sub>2</sub> and suggested that their presence could be indicative of sulfides (McAdam et al., 2014). However, these studies focused on the high-temperature production of these gases. The work presented here focused on low temperature evolutions of COS and CS<sub>2</sub> as well as the gases' relationships to SO<sub>2</sub>, CO<sub>2</sub>, and MTBSTFA (using BSW as a proxy). On their own, COS and CS<sub>2</sub> are the strongest discriminators among the five variables used. However, important information is contained within the relationships among the variables. SO<sub>2</sub> evolved at the temperatures analyzed can have mineralogical contributions from oxidized sulfides/elemental sulfur, iron sulfides, and/or iron sulfates. The relative amounts of COS and CS<sub>2</sub> compared to SO<sub>2</sub> play important roles in the QDA. Samples with similar amounts of COS and CS<sub>2</sub>, but different amounts of SO<sub>2</sub> are likely to be classified differently. The samples with more SO<sub>2</sub> are less likely to be classified with the sulfides. This is notably exemplified with the different classifications of HF/RH and DU/ST. More COS and CS<sub>2</sub> evolved relative to SO<sub>2</sub> in HF and RH than in DU and ST. The four samples also spanned a range of evolved BSW, indicating that production of COS and CS<sub>2</sub> was not a clear function of MTBSTFA presence. RH and HF have among the lowest and highest integrated counts of BSW, respectively, but they were both classified as likely to contain reduced sulfur while ST and DU had high BSW and were not likely to include reduced sulfur. This underscores the importance of the

relationships among all of the variables. High BSW alone is not enough to disqualify a sample from classification with reduced S.  $\text{CO}_2$  was higher for HF and RH than DU and ST, possibly acting as a source of carbon for the COS and  $\text{CS}_2$ .

#### 4.5.2. Classification of Samples With Previously Identified Sulfides

John Klein, Cumberland, and Oudam have previously been reported as having isotopic and/or XRD evidence consistent with the presence of sulfides. While JK and CB clustered with the sulfides in the QDA, OU did not. The posterior probability of JK clustering with the sulfides was 52%, which is lower than the other samples that clustered with the sulfides. John Klein was reported to contain small amounts of pyrrhotite (1.0 wt.%) and pyrite (0.3 wt.%) by CheMin (Vaniman et al., 2014), though these amounts were at or below the instrument's detection limit, which is 1 and 2 wt.% (Bish et al., 2013). Follow-up analysis of the CheMin data has not indicated the presence of sulfides in John Klein (Morrison et al., 2018). Likewise, reported isotopic evidence suggested that John Klein's  $\text{SO}_2$  evolution was not derived from sulfide (Franz et al., 2017). Cumberland, a nearby drilled sample from the same Sheepbed Mudstone as John Klein, did cluster with sulfides in the QDA with a high posterior probability of 89%. Like John Klein, pyrrhotite was originally reported by CheMin near the detection limit at 1.0 wt.% (Vaniman et al., 2014). The iron sulfide was similarly not reported in follow-up work (Morrison et al., 2018). However, unlike John Klein, sulfur isotopic evidence did suggest the presence of reduced sulfur in Cumberland (Franz et al., 2017). Taking this previous evidence into account with the EGA curves (Figure 1) and the results of the QDA, Cumberland is the strongest contender for having a reduced sulfur presence.

Oudam (OU) is a drilled sample from a Murray Formation mudstone. While there have been no reports of crystalline sulfides above CheMin detection limits, sulfur isotopes have indicated the possible presence of reduced sulfur in OU (Franz et al., 2017). There are two possible explanations for the mixed results. OU could be a false negative result in the QDA and actually contain some reduced sulfur. Alternatively, OU may have once had sulfides that were subsequently completely oxidized, but maintained the sulfidic isotopic signature. This latter scenario would align with the CheMin and QDA results. The results of these samples underscore the importance of using all information available from different sources in determining the likelihood of the presence of reduced sulfur.

#### 4.5.3. Implications for Vera Rubin Ridge

The results of the QDA indicate the presence of trace and/or amorphous sulfide in HF and RH, which are both samples of the Jura member on VRR. This in contrast to the nearby samples, ST (Pettegrove Point member on VRR) and DU (Blunts Point member stratigraphically below VRR), which were not identified in the QDA as containing reduced sulfur. The QDA classifications of these four samples are consistent with the samples' EGA profiles in Figure 1. This difference in sulfide presence between the stratigraphic members is indicative of differences between Jura and the rest of VRR/near-ridge rocks. Crystalline sulfides were not detected by CheMin in any of these four samples. Thus, the identification of sulfide in HF and RH necessitates that they are either amorphous, S-bearing organics (e.g., methyl sulfides or thiophenes, which have previously been observed on Mars; Eigenbrode et al., 2018), or below the CheMin detection limit. It is likely that the sulfides are at a trace level given the low integrated counts of sulfur volatiles in the EGA.

The likely presence of reduced sulfur in the Jura member of VRR adds to the complexity of the ridge's diagenetic history. Other observations also require explanation, such as the mobility of manganese, presence of jarosite, and color variations in VRR features. Figure 5 shows images of samples on Mars that demonstrate a range of possible alteration effects. Figures 5a–5d are the four drills holes of the (near) VRR samples: DU, ST, HF, and RH. Notably, Figure 5c shows an example of “gray” Jura member (HF), compared to the other, “red” VRR samples. Other parts of the Murray also show color variations likely caused by diagenetic fluids, as shown in Third Lake in Figure 5e. Third Lake shows a distinct red/gray color boundary in the block where the gray coloring appears to be associated with the white sulfate veins. Diagenetic fluids that followed the vein fractures likely altered the rock. Similarly, Figure 5f shows evidence of vein-associated alteration. This ChemCam Remote Micro-Imager of a Jura member target, Laphroaig, shows rod-like iron oxide “sticks” that indicate the occurrence of iron mobilization.

Several models have been proposed to explain the ridge's ancient diagenetic history and its timing (Fraeman et al., 2020). Here, we suggest an alternative model that can explain the observations of diagenetic features and presence of reduced sulfur on VRR. We propose that hematite formation was syndepositional and can account for the red coloring. Third Lake (Figure 5e), though not on VRR, suggests that red hematite may



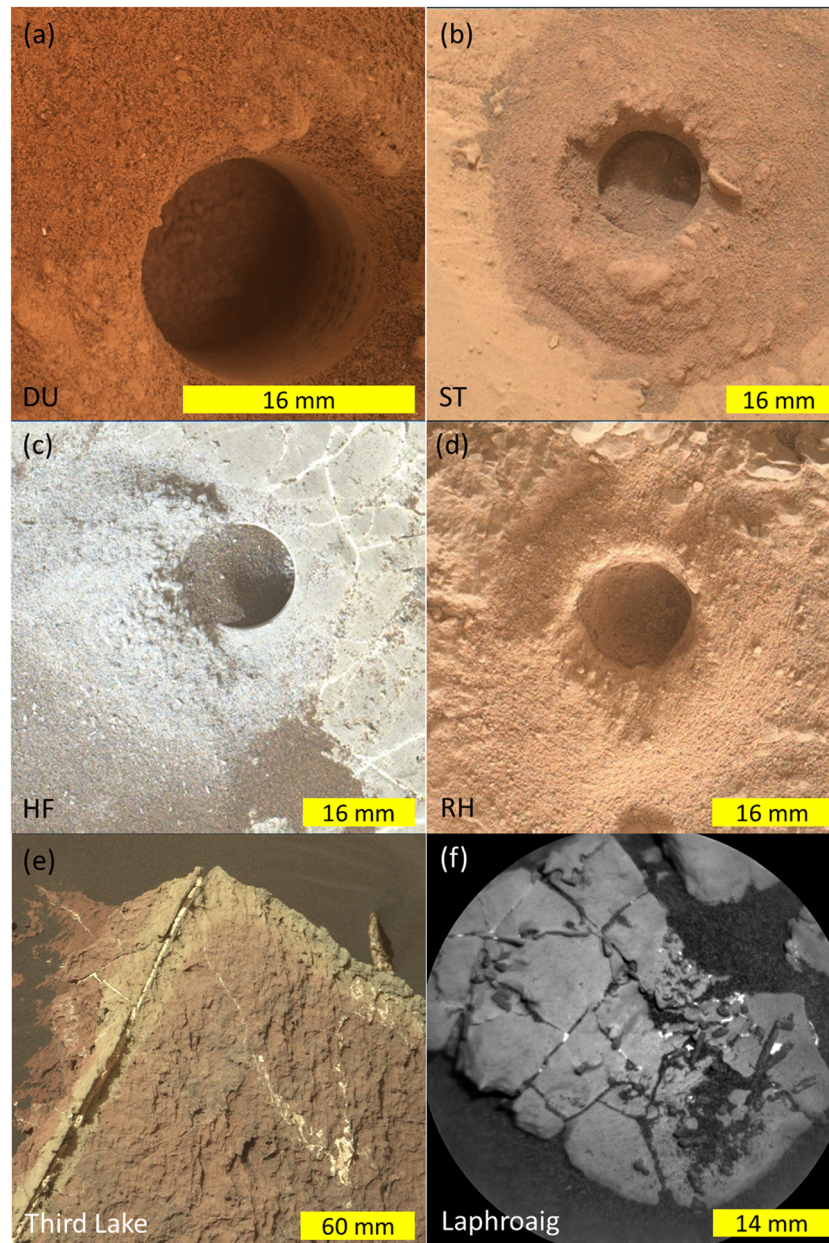


**Figure 5.** (a–d) MAHLI images of the four (near) VRR samples. Drill hole diameter is ~16 mm. (e) A Mastcam image of a Murray Formation bedrock block, Third Lake, that shows a color transition. (f) An image from the ChemCam Remote Micro-Imager of a Jura member target focusing on “sticks,” which are linear iron oxide features. Image identifiers: (a) 2082MH0001220010802084C00, (b) 2154MH0004650010802746C00, (c) 2247MH0004240010803292C00, (d) 2288MH0004240010803600C00, (e) 1612MR0082450010801054E02, (f) CR0\_566520230PRC\_F0671358CCAM03904L1. Credits (a–e) NASA/JPL-Caltech/MSSS, credits (f) NASA/JPL-Caltech/LANL.

be from primary deposition and later alteration. Sulfite-containing groundwater produced from  $\text{SO}_2$  dissolution (Halevy et al., 2007; Halevy & Schrag, 2009) could have flowed under a proto-Mt. Sharp. This fluid followed the diagenetic front observed by both Mn enrichments on VRR suggesting downward mobility (Frydenvang et al., 2020) and the ridge apparently conforming to the outline of the proto-Mt. Sharp. Similarly, the iron oxide “sticks” at Laphroaig (Figure 5f) suggest that iron was mobile in the water. Sulfite can reduce ferric iron from hematite (Palandri et al., 2005) and result in magnetite production. This magnetite would then be re-oxidized, likely by oxidants such as nitrates (Dhokal et al., 2013) or oxychlorine phases (such as chlorate; Mitra & Catalano, 2019), which appear to have been preserved in RH (McAdam et al., 2020). The resulting oxidized mineral phase would be martite, a



pseudomorph of magnetite that is identical to specular hematite in XRD and can account for the gray patches observed on VRR. The reduced sulfur identified in the Jura samples in this work could, in principle, be directly derived from the decomposition/disproportionation of some of the diagenetic sulfite (Matsuzaki et al., 1978; Pryor, 1960). Alternatively, the sulfite could have reacted with preexisting organic material forming organosulfur compounds. A reduced, mineral-bound organosulfur compound may have had a greater chance at preservation than an unbound sulfide (Keil & Mayer, 2013). This “sulfite model” explains the observations on VRR without requiring strongly reducing or hydrothermal fluids.

The presence of reduced sulfur in the Jura member of VRR has important implications for the potential habitability of the ridge. Reduced sulfur, in the form of trace crystalline metal sulfides, amorphous sulfides, or organosulfur compounds, could have supported sulfur-oxidizing metabolisms of a possible Martian microbial community. On Earth, various microorganisms have been described as iron sulfide oxidizers depending on Eh and pH conditions. For example, *Metallogenium gen.*, *Acidithiobacillus ferrooxidans*, *Sphaerotilus natans*, and *Gallionella ferruginea* have been reported as iron sulfide oxidizers in the pH ranges between 2 and 5 (Walsh & Mitchell, 1972a, 1972b) and 6 to 9 (Ralph, 1979). Under anaerobic conditions nitrate is the main electron acceptor used for sulfide oxidation by *Acidithiobacillus denitrificans* and *Sulfurimonas denitrificans* (Bosch et al., 2012; Poser et al., 2014). With reduced sulfur in VRR cooccurring with various oxidized species, such as nitrate in RH (McAdam et al., 2019), an energetic barrier to habitability is lifted. Given the once-present diagenetic fluids flowing through the rocks of VRR and likely presence of organic carbon, the conditions supported a habitable environment.

## 5. Conclusions

This work provides the first detailed analysis determining the presence of sulfides in Martian drilled samples using COS and CS<sub>2</sub> observed during evolved gas analysis. Using SAM-like EGA with sulfate and sulfide mixtures, we developed a set of training data for QDA. Using COS, CS<sub>2</sub>, SO<sub>2</sub>, CO<sub>2</sub>, and BSW evolved below 600°C in both the training data and Mars data, the QDA classified various Martian samples based on their likelihood of containing reduced sulfur. Two samples, John Klein and Cumberland, were classified as likely to contain sulfide, which is consistent with previously reported evidence and serves as a positive control for the QDA. On VRR, the Jura member samples, Highfield and Rock Hall, were identified as likely to contain reduced sulfur, while the two stratigraphically lower samples were not. Trace and/or amorphous sulfide in the Jura samples could be explained by several possible alteration models for VRR, including the “sulfite model” described here.

## Data Availability Statement

Original SAM data are publicly available in the Planetary Data System (<http://pds-geosciences.wustl.edu/missions/msl/>). The laboratory data used in this work are available on Harvard Dataverse, doi:10.7910/DVN/UOURYF (Wong, 2020).

## Acknowledgments

We thank the Mars Science Laboratory and Sample Analysis at Mars teams for their dedicated work operating the mission as well as their support in data collection, analyses, and discussions. G. M.W., A.C.M., J.L.E., and C.H.H. acknowledge the NASA Mars Exploration Program for providing support through the MSL Participating Scientist Program. G.M.W. acknowledges support of a NASA Earth and Space Science Fellowship. J. M.T.L. acknowledges support from the NASA Postdoctoral Program. R.N.G. acknowledges the support of Universidad Nacional Autónoma de México (UNAM: PAPIIT IN111619 and PAPIME PE102319). We also thank two anonymous reviewers for their valuable input in significantly improving this manuscript.

## References

- Altman, E. I., & Loris, B. (1976). A financial early warning system for over-the-counter broker-dealers. *The Journal of Finance*, 31(4), 1201–1217. <https://doi.org/10.2307/2326283>
- Archer, P. D. Jr., Franz, H. B., Sutter, B., Arevalo, R. D. Jr., Coll, P., Eigenbrode, J. L., et al. (2014). Abundances and implications of volatile-bearing species from evolved gas analysis of the Rocknest aeolian deposit, Gale crater, Mars. *Journal of Geophysical Research: Planets*, 119, 237–254. <https://doi.org/10.1002/2013JE004493>
- Arutyunov, V. S. (1992). The kinetics of gas-phase processes in systems containing carbon and sulphur. *Russian Chemical Reviews*, 61(11), 1140–1155. <https://doi.org/10.1070/rc1992v061n11abeh001022>
- Attar, A. (1978). Chemistry, thermodynamics and kinetics of reactions of sulphur in coal-gas reactions: A review. *Fuel*, 57(4), 201–212. [https://doi.org/10.1016/0016-2361\(78\)90117-5](https://doi.org/10.1016/0016-2361(78)90117-5)
- Bhargava, S. K., Garg, A., & Subasinghe, N. D. (2009). In situ high-temperature phase transformation studies on pyrite. *Fuel*, 88, 988–993. <https://doi.org/10.1016/j.fuel.2008.12.005>
- Bish, D. L., Blake, D. F., Vaniman, D. T., Chipera, S. J., Morris, R. V., Ming, D. W., et al. (2013). X-ray diffraction results from Mars Science Laboratory: Mineralogy of Rocknest at Gale crater. *Science*, 341, 1238932. <https://doi.org/10.1126/science>
- Blake, D., Vaniman, D., Achilles, C., Anderson, R., Bish, D., Bristow, T., et al. (2012). Characterization and calibration of the CheMin mineralogical instrument on Mars Science Laboratory. *Space Science Reviews*, 170, 341–399. <https://doi.org/10.1007/s11214-012-9905-1>
- Bosch, J., Lee, K.-Y., Jordan, G., Kim, K.-W., & Meckenstock, R. U. (2012). Anaerobic, nitrate-dependent oxidation of pyrite nanoparticles by *Thiobacillus denitrificans*. *Environmental Science & Technology*, 46, 2095–2101. <https://doi.org/10.1021/es2022329>
- Conrad, P. G., Eigenbrode, J. L., von der Heydt, M. O., Mogensen, C. T., Canham, J., Harpold, D. N., et al. (2012). The Mars Science Laboratory organic check material. *Space Science Reviews*, 170, 479–501. <https://doi.org/10.1007/s11214-012-9893-1>

- Dhakal, P., Matocha, C. J., Huggins, F. E., & Vandiviere, M. M. (2013). Nitrite reactivity with magnetite. *Environmental Science & Technology*, *47*, 6206–6213. <https://doi.org/10.1021/es304011w>
- Driscoll, R. L., & Leinz, R. W. (2005). Methods for Synthesis of Some Jarosites: U.S Geological Survey Techniques and Methods 5-D1. Reston, VA.
- Duan, L., Zhao, C., Zhou, W., Qu, C., & Chen, X. (2009). Investigation on coal pyrolysis in CO<sub>2</sub> atmosphere. *Energy & Fuels*, *23*, 3826–3830. <https://doi.org/10.1021/ef9002473>
- Eigenbrode, J. L., Summons, R. E., Steele, A., Freissinet, C., Millan, M., Navarro-González, R., et al. (2018). Organic matter preserved in 3-billion-year-old mudstones at Gale crater, Mars. *Science*, *360*, 1096–1101. <https://doi.org/10.1126/science.aas9185>
- Fedo, C., Grotzinger, J. P., Gupta, S., Banham, S., Bennett, K., Edgar, L., ... Vasavada, A. R. (2019). Evidence for Persistent, Water-Rich, Lacustrine Deposition Preserved in the Murray Formation, Gale Crater: A Depositional System Suitable for Sustained Habitability. In *Ninth International Conference on Mars*.
- Finch, W. H., & Schneider, M. K. (2006). Misclassification rates for four methods of group classification: Impact of predictor distribution, covariance inequality, effect size, sample size, and group size ratio. *Educational and Psychological Measurement*, *66*, 240–257. <https://doi.org/10.1177/0013164405278579>
- Fraeman, A. A., Arvidson, R. E., Catalano, J. G., Grotzinger, J. P., Morris, R. V., Murchie, S. L., et al. (2013). A hematite-bearing layer in Gale crater, Mars: Mapping and implications for past aqueous conditions. *Geology*, *41*, 1103–1106. <https://doi.org/10.1130/G34613.1>
- Fraeman, A. A., Edgar, L. A., Rampe, E. B., Thompson, L. M., Frydenvang, J., Fedo, C. M., et al. (2020). Evidence for a diagenetic origin of Vera Rubin ridge, Gale crater, Mars: Summary and synthesis of Curiosity's exploration campaign. *Journal of Geophysical Research: Planets*, *125*, e2020JE006527. <https://doi.org/10.1029/2020JE006527>
- Fraeman, A. A., Ehlmann, B. L., Arvidson, R. E., Edwards, C. S., Grotzinger, J. P., Milliken, R. E., et al. (2016). The stratigraphy and evolution of lower mount sharp from spectral, morphological, and thermophysical orbital data sets. *Journal of Geophysical Research: Planets*, *121*, 1713–1736. <https://doi.org/10.1002/2016JE005095>
- Franz, H. B., McAdam, A. C., Ming, D. W., Freissinet, C., Mahaffy, P. R., Eldridge, D. L., et al. (2017). Large sulfur isotope fractionations in Martian sediments at Gale crater. *Nature Geoscience*, *10*, 658–662. <https://doi.org/10.1038/ngeo3002>
- Freissinet, C., Glavin, D. P., Buch, A., Szopa, C., Teinturier, S., Archer, P. D. J., ... Mahaffy, P. R. (2019). Detection of Long-Chain Hydrocarbons on Mars with the Sample Analysis at Mars (SAM) Instrument. In *Ninth International Conference on Mars*. Pasadena, CA: Lunar and Planetary Institute. Retrieved from <http://www.lpi.usra.edu/meetings/ninthmars2019/pdf/6123.pdf>
- Freissinet, C., Glavin, D. P., Mahaffy, P. R., Miller, K. E., Eigenbrode, J. L., Summons, R. E., et al. (2015). Organic molecules in the Sheepbed mudstone, Gale crater, Mars. *Journal of Geophysical Research: Planets*, *120*, 495–514. <https://doi.org/10.1002/2014JE004737>
- Frigge, L., Elserafi, G., Ströhle, J., & Epple, B. (2016). Sulfur and chlorine gas species formation during coal pyrolysis in nitrogen and carbon dioxide atmosphere. *Energy & Fuels*, *30*, 7713–7720. <https://doi.org/10.1021/acs.energyfuels.6b01080>
- Frydenvang, J., Mangold, N., Wiens, R. C., Fraeman, A. A., Edgar, L., Fedo, C., ... Salvatore, M. (2019). The Role of Large-Scale Diagenesis in the Formation of Vera Rubin Ridge in Gale Crater, Mars, as Implied by ChemCam Observations. In *50th Lunar and Planetary Science Conference* (LPI Contrib. No. 2132). The Woodlands, TX.
- Frydenvang, J., Mangold, N., Wiens, R. C., Fraeman, A. A., Edgar, L. A., Fedo, C., et al. (2020). The chemostratigraphy of the Murray Formation and role of diagenesis at Vera Rubin Ridge in Gale Crater, Mars, as observed by the ChemCam instrument. *Journal of Geophysical Research: Planets*, *125*, e2019JE006320. <https://doi.org/10.1029/2019JE006320>
- Glavin, D. P., Freissinet, C., Miller, K. E., Eigenbrode, J. L., Brunner, A. E., Buch, A., et al. (2013). Evidence for perchlorates and the origin of chlorinated hydrocarbons detected by SAM at the Rocknest aeolian deposit in Gale crater. *Journal of Geophysical Research: Planets*, *118*, 1955–1973. <https://doi.org/10.1002/jgre.20144>
- Grotzinger, J. P., Crisp, J., Vasavada, A. R., Anderson, R. C., Baker, C. J., Barry, R., et al. (2012). Mars Science laboratory Mission and Science investigation. *Space Science Reviews*, *170*, 5–56. <https://doi.org/10.1007/s11214-012-9892-2>
- Grotzinger, J. P., & Milliken, R. E. (2012). The sedimentary rock record of Mars: Distribution, origins, and global stratigraphy. In J. P. Grotzinger, & R. E. Milliken (Eds.), *Sedimentary geology of Mars* (Vol. 102, pp. 1–48). Tulsa, OK: SEPM Special Publication. <https://doi.org/10.2110/pec.12.102.0001>
- Grotzinger, J. P., Sumner, D. Y., Kah, L. C., Stack, K., Gupta, S., Edgar, L., et al. (2014). A habitable fluvio-lacustrine environment at Yellowknife Bay, Gale crater, Mars. *Science*, *343*, 1242777. <https://doi.org/10.1126/science>
- Halevy, I., & Schrag, D. P. (2009). Sulfur dioxide inhibits calcium carbonate precipitation: Implications for early Mars and Earth. *Geophysical Research Letters*, *36*, L23201. <https://doi.org/10.1029/2009GL040792>
- Halevy, I., Zuber, M. T., & Schrag, D. P. (2007). A sulfur dioxide climate feedback on early Mars. *Science*, *318*(5858), 1903–1907. <https://doi.org/10.1126/science.1147039>
- Härdle, W. K., & Simar, L. (2015a). Discriminant analysis. In *Applied multivariate statistical analysis* (pp. 407–424). Berlin, Heidelberg: Springer. <https://doi.org/10.1007/978-3-662-45171-7>
- Härdle, W. K., & Simar, L. (2015b). Principal components analysis. In *Applied multivariate statistical analysis* (pp. 319–358). Berlin, Heidelberg: Springer. <https://doi.org/10.1007/978-3-662-45171-7>
- Horgan, B., Fraeman, A., Johnson, J. R., Thompson, L., Jacob, S., Wellington, D., ... Grotzinger, J. (2019). Redox conditions during diagenesis in the Vera Rubin ridge, Gale crater, Mars from Mastcam multispectral images. In *50th Lunar and Planetary Science Conference* (LPI Contrib. No. 2132).
- Hunter, J. D. (2007). Matplotlib: A 2D graphics environment. *Computing in Science & Engineering*, *9*, 90–95. <https://doi.org/10.1109/MCSE.2007.55>
- Keil, R. G., & Mayer, L. M. (2013). Mineral matrices and organic matter. In *Treatise on geochemistry* (2nd ed., Vol. 12, pp. 337–359). New York, NY: Elsevier Ltd. <https://doi.org/10.1016/B978-0-08-095975-7.01024-X>
- Knudson, C. A., Perrett, G. M., McAdam, A. C., Campbell, J. L., Sargent, L., Flannigan, E. L., ... Mahaffy, P. R. (2018). Investigation of Mineral Phase Effects (MPEs) Caused by Sulfur Bearing Minerals in the Cumberland Simulant, Using Laboratory Equivalents of SAM, APXS, and CheMin Mars Science Laboratory (MSL) Instruments. Washington, DC: AGU Fall Meeting Abstracts.
- Leshin, L. A., Mahaffy, P. R., Webster, C. R., Cabane, M., Coll, P., Conrad, P. G., et al. (2013). Volatile, isotope, and organic analysis of martian fines with the Mars Curiosity rover. *Science*, *341*, 1238937. <https://doi.org/10.1126/science>
- Mahaffy, P. R., Webster, C. R., Cabane, M., Conrad, P. G., Coll, P., Atreya, S. K., et al. (2012). The sample analysis at Mars investigation and instrument suite. *Space Science Reviews*, *170*, 401–478. <https://doi.org/10.1007/s11214-012-9879-z>
- Malespin, C. A., Johnson, C., Arealo, R., Brinckerhoff, W., McAdam, A. C., Teinturier, S., ... Mahaffy, P. R. (2016). Mars environment chambers in NASA Goddard's planetary environments lab. In *47th lunar and planetary Science Conference*. The Woodlands, TX.

- Matsuzaki, R., Masumizu, H., Murakami, N., & Saeki, Y. (1978). The thermal decomposition process of calcium sulfite. *Bulletin of the Chemical Society of Japan*, 51(1), 121–122. <https://doi.org/10.1246/bcsj.51.121>
- McAdam, A. C., Franz, H. B., Sutter, B., Archer, P. D. Jr., Freissinet, C., Eigenbrode, J. L., et al. (2014). Sulfur-bearing phases detected by evolved gas analysis of the Rocknest aeolian deposit, Gale crater, Mars. *Journal of Geophysical Research: Planets*, 119, 373–393. <https://doi.org/10.1002/2013JE004518>
- McAdam, A. C., Sutter, B., Archer, P. D., Franz, H. B., Eigenbrode, J. L., Stern, J. C., ... Mahaffy, P. R. (2019). Constraints on the Chemistry and Mineralogy of the Clay-Bearing Unit from Sample Analysis at Mars Evolved Gas Analyses. In *Ninth International Conference on Mars*. Pasadena, CA: Lunar and Planetary Institute. Retrieved from <http://www.lpi.usra.edu/meetings/ninthmars2019/pdf/6131.pdf>
- McAdam, A. C., Sutter, B., Archer, P. D., Franz, H. B., Wong, G. M., Lewis, J. M. T. et al. (2020). Constraints on the mineralogy and geochemistry of the Vera Rubin ridge, Gale crater, Mars from Mars Science Laboratory Sample Analysis at Mars Evolved Gas Analysis. *Journal of Geophysical Research: Planets*, 125, e2019JE006309. <https://doi.org/10.1029/2019JE006309>
- McKinney, W. (2010). Data structures for statistical computing in Python. In *Proceedings of the 9th Python in Science Conference* (pp. 51–56).
- Millan, M., Malespin, C. A., Freissinet, C., Glavin, D. P., Mahaffy, P. R., Buch, A., ... Johnson, S. S. (2019). Lessons Learned from the Full Cup Wet Chemistry Experiment Performed on Mars with the Sample Analysis at Mars Instrument. Pasadena, California: Ninth International Conference on Mars 2019.
- Milliken, R. E., Grotzinger, J. P., & Thomson, B. J. (2010). Paleoclimate of Mars as captured by the stratigraphic record in Gale crater. *Geophysical Research Letters*, 37, L04201. <https://doi.org/10.1029/2009GL041870>
- Ming, D. W., Archer, P. D., Glavin, D. P., Eigenbrode, J. L., Franz, H. B., Sutter, B., et al. (2014). Volatile and organic compositions of sedimentary rocks in Yellowknife. *Science*, 343, 1245267. <https://doi.org/10.1126/science>
- Mitra, K., & Catalano, J. G. (2019). Chlorate as a potential oxidant on Mars: Rates and products of dissolved Fe (II) oxidation. *Journal of Geophysical Research: Planets*, 124, 2893–2916. <https://doi.org/10.1029/2019JE006133>
- Morrison, S. M., Downs, R. T., Blake, D. F., Vaniman, D. T., Ming, D. W., Hazen, R. M., et al. (2018). Crystal chemistry of Martian minerals from Bradbury landing through Naukluft Plateau, Gale crater, Mars. *American Mineralogist*, 103, 857–871. <https://doi.org/10.2138/am-2018-6124>
- Myers, L., & Siros, M. J. (2006, August 15). Spearman Correlation Coefficients, Differences between. *Encyclopedia of Statistical Sciences*. <https://doi.org/10.1002/0471667196.ess5050.pub2>
- NIST Mass Spectrometry Data Center, & Wallace, W. E. (Director). (2018). Mass spectra. In P. J. Linstrom & W. G. Mallard (Eds.), *NIST Chemistry WebBook, NIST Standard Reference Database Number 69*. Gaithersburg, MD.
- Palandri, J. L., Rosenbauer, R. J., & Kharaka, Y. K. (2005). Ferric iron in sediments as a novel CO<sub>2</sub> mineral trap: CO<sub>2</sub>-SO<sub>2</sub> reaction with hematite. *Applied Geochemistry*, 20, 2038–2048. <https://doi.org/10.1016/j.apgeochem.2005.06.005>
- Pedregosa, F., Varoquaux, G., Gramfort, A., Michel, V., Thirion, B., Grisel, O., et al. (2011). Scikit-learn: Machine learning in Python. *Journal of Machine Learning Research*, 12, 2825–2830.
- Poser, A., Vogt, C., Knöller, K., Ahlheim, J., Weiss, H., Kleinsteuber, S., & Richnow, H.-H. (2014). Stable sulfur and oxygen isotope fractionation of anoxic sulfide oxidation by two different enzymatic pathways. *Environmental Science & Technology*, 48, 9094–9102. <https://doi.org/10.1021/es404808r>
- Pryor, W. A. (1960). The kinetics of the disproportionation of sodium thiosulfate to sodium sulfide and sulfate. *Journal of the American Chemical Society*, 82(18), 4794–4797. <https://doi.org/10.1021/ja01503a010>
- Ralph, B. J. (1979). Oxidative reactions in the sulfur cycle. In P. A. Trudinger, & D. J. Swaine (Eds.), *Biochemical cycling of mineral-forming elements* (pp. 369–400). New York, NY: Elsevier. [https://doi.org/10.1016/S0166-1116\(08\)71064-1](https://doi.org/10.1016/S0166-1116(08)71064-1)
- Shao, D., Hutchinson, E. J., Heidbrink, J., Pan, W.-P., & Chou, C.-L. (1994). Behavior of sulfur during coal pyrolysis. *Journal of Analytical and Applied Pyrolysis*, 30(1), 91–100. [https://doi.org/10.1016/0165-2370\(94\)00807-8](https://doi.org/10.1016/0165-2370(94)00807-8)
- Stern, J. C., Graham, H., McAdam, A., Knudson, C. A., Morris, R. V., Lasue, J., ... Mahaffy, P. R. (2018). Characterization and Development of a Mineralogical and Chemical Analog of Cumberland Drill Sample Sediments for Organic Molecule Identification in Evolved Gas Analysis Experiments. In *AGU Fall Meeting Abstracts*. Washington, DC.
- Stern, J. C., McAdam, A. C., Ten Kate, I. L., Bish, D. L., Blake, D. F., Morris, R. V., et al. (2013). Isotopic and geochemical investigation of two distinct Mars analog environments using evolved gas techniques in Svalbard, Norway. *Icarus*, 224, 297–308. <https://doi.org/10.1016/j.icarus.2012.07.010>
- Stern, J. C., Sutter, B., Archer, P. D., Eigenbrode, J. L., McAdam, A. C., Franz, H. B., et al. (2018). Major volatiles evolved from Eolian materials in Gale crater. *Geophysical Research Letters*, 45, 10,240–10,248. <https://doi.org/10.1029/2018GL079059>
- Sutter, B., McAdam, A. C., Mahaffy, P. R., Ming, D. W., Edgett, K. S., Rampe, E. B., et al. (2017). Evolved gas analyses of sedimentary rocks and eolian sediment in Gale crater, Mars: Results of the curiosity rover's sample analysis at Mars instrument from Yellowknife Bay to the Namib dune. *Journal of Geophysical Research: Planets*, 122, 2574–2609. <https://doi.org/10.1002/2016JE005225>
- van der Walt, S., Colbert, S. C., & Varoquaux, G. (2011). The NumPy Array: A structure for efficient numerical computation. *Computing in Science & Engineering*, 13(2), 22–30. <https://doi.org/10.1109/MCSE.2011.37>
- Vaniman, D. T., Bish, D. L., Ming, D. W., Bristow, T. F., Morris, R. V., Blake, D. F., et al. (2014). Mineralogy of a mudstone at Yellowknife Bar, Gale crater, Mars. *Science*, 343, 1243480. <https://doi.org/10.1126/science.1243480>
- Virtanen, P., Gommers, R., Oliphant, T. E., Haberland, M., Reddy, T., Cournapeau, D., ... Contributors, S. 1. 0. (2019). SciPy 1.0--Fundamental Algorithms for Scientific Computing in Python.
- Walsh, F., & Mitchell, R. (1972a). An acid-tolerant iron-oxidizing metallogenium. *Journal of General Microbiology*, 72(2), 369–376. <https://doi.org/10.1099/00221287-72-2-369>
- Walsh, F., & Mitchell, R. (1972b). pH-dependent succession of iron bacteria. *Environmental Science & Technology*, 6(9), 809–812. <https://doi.org/10.1021/es60068a001>
- Wang, B., Zhao, S., Huang, Y., & Zhang, J. (2014). Effect of some natural minerals on transformation behavior of sulfur during pyrolysis of coal and biomass. *Journal of Analytical and Applied Pyrolysis*, 105, 284–294. <https://doi.org/10.1016/j.jaap.2013.11.015>
- Wang, X., Li, X., Ma, R., Li, Y., Wang, W., Huang, H., et al. (2018). Quadratic discriminant analysis model for assessing the risk of cadmium pollution for paddy fields in a county in China. *Environmental Pollution*, 236, 366–372. <https://doi.org/10.1016/j.envpol.2018.01.088>
- Wong, G. (2020). Processed data for figures and analysis in “Detection of reduced sulfur on Vera Rubin ridge by quadratic discriminant analysis of volatiles observed during evolved gas analysis.” Harvard Dataverse. <https://doi.org/10.7910/DVN/UOURYF>
- Wray, J. J. (2013). Gale crater: The Mars Science Laboratory/Curiosity rover landing site. *International Journal of Astrobiology*, 12(1), 25–38. <https://doi.org/10.1017/S1473550412000328>
- Zhang, M. Q. (1997). Identification of protein coding regions in the human genome by quadratic discriminant analysis. *Proceedings of the National Academy of Sciences*, 94(2), 565–568. <https://doi.org/10.1073/pnas.94.2.565>